

Editorial Manager(tm) for Photosynthesis Research
Manuscript Draft

Manuscript Number:

Title: X-ray structure of Rhodobacter capsulatus cytochrome bc1: Comparison with its mitochondrial and chloroplast counterparts

Article Type: Special Issue (ALLEN/KNAFF)

Section/Category:

Keywords: cytochrome bc1, respiration, photosynthesis, electron transport, X-ray structure

Corresponding Author: Edward A Berry Lawrence Berkeley National Lab

First Author: Edward A Berry, Ph.D.

Order of Authors: Edward A Berry, Ph.D.; Li-Shar Huang, Ph.D.; Lai K Saechao; Ning G Pon, Ph.D.; Maria Valkova-Valchanova; Fevzi Daldal, Ph.D

Abstract:

X-ray structure of *Rhodobacter capsulatus* cytochrome *bc₁*: Comparison with its mitochondrial and chloroplast counterparts

Edward A. Berry^{1*}, Li-Shar Huang¹, Lai K. Saechao¹, Ning. G. Pon¹
Maria Valkova-Valchanova^{2#} and Fevzi Daldal^{2*}

¹Lawrence Berkeley National Laboratory, 1 Cyclotron road, Berkeley CA 94720

²University of Pennsylvania, Department of Biology, Philadelphia, PA 19104-6018

Running title: *Rhodobacter capsulatus* cyt *bc₁* structure

keywords: cytochrome *bc₁*, respiration, photosynthesis, electron transport, X-ray structure

*corresponding authors: E. A. Berry: phone: 510- 486-4335; EABerry@LBL.gov
F. Daldal: phone: 215-898-4394; fdaldal@sas.upenn.edu

#Present address: Medarex, Inc. Bloomsbury, NJ 08804

Abstract

Ubihydroquinone: cytochrome (cyt) *c* oxidoreductase, or cyt *bc*₁, is a widespread, membrane integral enzyme that plays a crucial role during photosynthesis and respiration. It is one of the major contributors of the electrochemical proton gradient, which is subsequently used for ATP synthesis. The simplest form of the cyt *bc*₁ is found in bacteria, and it contains only the three ubiquitously conserved catalytic subunits: the FeS protein, cyt *b* and cyt *c*₁. Here we present a preliminary X-ray structure of *Rhodobacter capsulatus* cyt *bc*₁, and compare it to the available structures of its homologues from mitochondria and chloroplast. Using the bacterial enzyme structure, we highlight the structural similarities and differences that are found among the three catalytic subunits between the members of this family of enzymes. In addition, we discuss the locations of currently known critical mutations, and their implications in terms of the cyt *bc*₁ catalysis.

Introduction

The ubiquinol : cytochrome (cyt) *c* oxidoreductase (or cyt *bc₁*), is a multi subunit membrane integral enzyme encountered in a broad variety of prokaryotic and eukaryotic organisms (for reviews see (Berry et al. 2000; Darrouzet et al. 2001; Cramer et al. 2004; Darrouzet et al. 2004)). While the mitochondrial and bacterial enzymes are referred to as cyt *bc₁*, the homologous enzyme in plant and algal chloroplasts and cyanobacteria is called plastoquinone : plastocyanin oxidoreductase or cyt *b₆f* (for a review see Cramer et al. 1996; Cramer et al. 2004). In all cases, these energy transducing enzymes transfer electrons from a hydroquinone derivative (QH₂) (usually ubiquinol, menaquinone or plastoquinone), to an electron carrier molecule such as a *c* type cyt, a high potential iron sulfur protein (HiPIP) or a plastocyanin ((Jenney and Daldal 1993; Jenney et al. 1994; Hochkoeppler et al. 1996; Kerfeld et al. 1996)). They are central players in respiration and photosynthesis as they contribute to the generation of an electrochemical potential $\Delta\mu\text{H}^+$, subsequently used for ATP production via the ATP synthase ((Mitchell 1976) (Saraste 1999) (Dutton, Moser et al. 1998)). Maintenance of an appropriate $\Delta\mu\text{H}^+$ is an essential process for all living cells, thus nearly all electron transport chains whose function is to develop a $\Delta\mu\text{H}^+$ contain a member of this family.

A typical bacterial cyt *bc₁* is constituted of three subunits (Yang and Trumpower 1986; Robertson et al. 1993), namely a high potential [2Fe2S] cluster containing iron-sulfur (FeS) protein, also called Rieske protein after its discoverer) (Rieske et al. 1964), a multi span integral membrane protein cyt *b* which has two *b*-type hemes (named *b_L* and *b_H*, for low and high redox mid point potential) located on the positive (P) and negative (N) sides, respectively, of energy transducing membranes, and a *c*-type cyt with a covalently attached heme, called cyt *c₁*. These three subunits form a monomer that dimerizes to yield an active cyt *bc₁* with two active sites per monomer, referred to as Q_o (hydroquinone (QH₂) oxidation)

and Q_i (quinone (Q) reduction) sites. The Q_o site, where QH_2 is oxidized to Q, is at the interface between the FeS protein and cyt *b* on the P side of the membrane, while the Q_i site, where Q is reduced to QH_2 , is confined solely to cyt *b* and is closer to the N side of the membrane.

The mechanism of redox coupled proton translocation by the cyt bc_1 is best described by the modified Q cycle mechanism (Mitchell 1976; Crofts and Meinhardt 1982; Crofts et al. 1983). According to this mechanism, the Q_o site of the cyt bc_1 oxidizes one QH_2 from the membrane Q_{p00l} , releases two protons, and conveys the two ensuing electrons into two different electron acceptor chains via a reaction called 'oxidant-induced reduction'. During this unique bifurcated electron transfer process, the first electron is delivered to the high potential chain formed of the 2Fe2S cluster of the FeS protein and the *c*-type heme of the cyt c_1 . From there it ultimately reaches via an electron carrier protein (*e. g.*, a *c*-type cyt) a terminal acceptor such as a cyt *c* oxidase during respiration, or a photochemical reaction center during photosynthesis. The second electron is conveyed via the heme b_L and heme b_H of cyt *b* to the Q_i site, where it reduces a Q to a stable semiquinone (SQ). Upon oxidation of a second QH_2 molecule via a second turnover of the Q_o site, the SQ at the Q_i site is converted to QH_2 and released back to the membrane Q_{p00l} . Therefore, the cyt bc_1 oxidizes overall one molecule of QH_2 to Q, reduces two electron carrier molecules, releases four protons to the P side, and takes up two protons from the N side of the energy transducing membrane. In this manner, it uses very efficiently a small ΔG that exists between its substrate QH_2 and its electron carrier protein to contribute to the establishment of both a pH gradient (ΔpH) and a trans membrane electrical charge separation ($\Delta \psi$) (Darrrouzet et al. 2001).

Currently, how the bifurcated electron transfer reaction that constitutes the essence of the energetic efficiency of the cyt bc_1 occurs, is not understood. In particular, whether

QH₂ oxidation at the Q_O site occurs via a “genuinely concerted” two-electron transfer mode that proceeds without any SQ intermediate (Osyczka et al. 2004), or via a sequential but “kinetically concerted” two one-electron transfer steps that take place via a highly unstable SQ is debated ((Crofts et al. 2000; Trumpower 2002). In any event, clearly Q_O site malfunction is an energetic disaster for living cells as it diminishes drastically the $\Delta\mu\text{H}^+$, hence the production of ATP, and yields large amounts of undesired reactive oxygen species (Darrouzet et al. 2001; Muller et al. 2002). Thus, to better understand these mechanistic issues, it is important to establish the high-resolution structure of a simple cyt *bc*₁ from bacteria such as *Rhodobacter* species that are readily amenable to sophisticated genetic manipulations.

A large part of the complexity of the mitochondrial cyt *bc*₁, which plays an identical electron transfer role as the bacterial enzyme, may be a result of endosymbiosis that has distributed the various components of this enzymes between organellar and nuclear genomes, consequently requiring their assembly from two different sources into the mitochondrial membrane (Zara et al. 2004). These additional complexities are absent in bacteria, rendering the interpretation of genetic results more straightforward. Indeed, a great deal of information is available concerning the effects of single, as well as compensatory pairs of point mutations on the assembly and function of *Rhodobacter* cyt *bc*₁ (Brasseur et al. 1996). While the interpretation of these data has been greatly aided by the availability of the mitochondrial structures (Xia et al. 1997; Iwata et al. 1998; Zhang et al. 1998; Hunte et al. 2000; Gao et al. 2003; Palsdottir et al. 2003), there are also important differences due to specific insertions and deletions that are uniquely present in the bacterial or mitochondrial enzymes.

Various three dimensional structures of the mitochondrial cyt *bc*₁, which have been accumulated during the last several years (Xia et al. 1997; Iwata et al. 1998; Zhang et al. 1998; Hunte et al. 2000; Gao et al. 2003; Palsdottir et al. 2003), have recently been supplemented by the structures of the cyt *b₆f* from cyanobacteria and chloroplast (Kurusu et al. 2003; Stroebel et al. 2003). Crystallization of the simpler bacterial cyt *bc*₁ has been

considerably more challenging, and the crystals obtained to date are not particularly satisfactory for structure determination due to high mosaicity as well as poor and anisotropic crystalline order. Nevertheless we have made some progress, and we expect eventually to have a structure at 3.5 Å or better. Here we report, as the first X-ray structure of a bacterial cyt *bc*₁, our model of the *Rhodobacter capsulatus* cyt *bc*₁ currently being refined against data from crystals diffracting anisotropically to around 3.5 Å, and compare it with its mitochondrial and chloroplast homologues to underline salient differences and similarities between these enzymes. In addition, using the *Rhodobacter* structure we visualize the location of various critical mutations that have been obtained in the past, and discuss their implications on the cyt *bc*₁ catalytic mechanism.

Materials and Methods

Stigmatellin was from Fluka, detergents from Anatrace, buffers and reagents from Sigma. Amino acid sequences were retrieved from the NCBI databases using BLAST (Altschul et al. 1997) and aligned with CLUSTALW at the "NPS@" web site (Combet et al. 2000). Figures were made using Molscript(Kraulis 1991), RasMol (Sayle and Milner-White 1995), and "O" (Jones et al. 1991).

Large-scale purification of *Rb. capsulatus* cyt *bc*₁. Cyt *bc*₁ was purified from the *Rb. capsulatus* strain pMTS1/MT-RBC1 that contains a deletion of the cyt *bc*₁ structural genes on the chromosome, complemented *in trans* with a wild type copy of these genes carried on a low copy plasmid (Gray, Dutton et al. 1994). This strain overproduces the cyt *bc*₁ by about five to eight fold when grown in enriched medium under semi-aerobic conditions. Intracytoplasmic membranes (chromatophores) were obtained by differential centrifugation after breaking the cells using a French press, as described earlier (Darrouzet, Valkova-Valchanova et al. 2000)

The cyt *bc*₁ was isolated by ion-exchange chromatography of a dodecyl maltoside extract, essentially as described (Berry et al. 1991). Specifically, chromatophore membranes were solubilized at 10 g/l protein in 50 mM potassium phosphate buffer (KPi) pH 7.3 containing 260 mM NaCl, 0.1 mM PMSF (added freshly from an ethanolic solution) and dodecyl-β-D-maltoside (DM) at a detergent:protein ratio of 1:1. The mixture was stirred for ~20 min and centrifuged for 30 min at 13500 x g. The supernate was passed through a 2.5 x 100 cm column of DEAE-Sepharose CL-6B equilibrated with 50 mM KPi, 260 mM NaCl, and 0.1 g/l DM. The column was then washed with one volume of the same buffer and then eluted with a gradient 500 + 500 ml 260 to 500 mM NaCl in 50 mM KPi with 0.1 g/l DM.

Pooled fractions were concentrated and applied to a Sepharose CL-6B column to isolate a monodisperse dimeric population of the cyt *bc*₁. Peak fractions from this column were pooled. Stigmatellin was added from a 10 mM stock solution (ethanolic) at a ratio of two molecules per cyt *bc*₁ monomer (based on an estimated extinction coefficient of 59 mM⁻¹ for the dithionite-reduced complex at 560 nm vs 600 nm). The sample was then concentrated by ultrafiltration to a few ml,

diluted with 20 mM Tris-HCl, 0.5 mM EDTA (crystallization buffer) and concentrated to around 200 μ M of cyt *bc*₁. This concentrated solution was supplemented with 1 g/l undecyl maltoside and appropriate additives just before droplets were set up for crystallization by mixing with precipitant solution as described below.

Early crystallization attempts resulted in three different crystal forms, with trigonal, tetragonal, and monoclinic lattices. All three had high mosaic spread (1.5-2.5 degrees) and diffraction was limited to 6-7 Å at first. Later improved monoclinic crystals were made diffracting to better than 3.5 Å, and the structure presented here is refined against the best of these.

Crystallization was by vapor diffusion in a sitting drop format. The most successful conditions were derived from Hampton Research membrane protein factorial (MF) #31. Crystals were obtained with 20 to 40% PEG 400, 100 mM MgCl₂ and 0.1 M Na cacodylate or citrate pH 5.1 to 6.0. For the crystal used in the final refinement, 30 μ l of protein in 20 mM Tris-HCl pH 7.5 + 0.5 mM EDTA was supplemented with 1 g/l undecyl maltoside and 15 g/l heptanetriol, and mixed with an equal volume of precipitant containing 0.1 M Na-cacodylate pH 5.1, 25% PEG-400, 0.1M MgCl, and 3 mM NaN₃. The tetragonal crystal was obtained with cacodylate buffer at pH 6.0, and the trigonal one with citrate at pH 5.2, however the factors affecting crystal form are not clear, and in at least one case two forms were observed growing together in the same well.

Data were collected at synchrotron light sources (the Advanced Light Source in Berkeley (ALS) and the Stanford Synchrotron Radiation Lab (SSRL). Crystals were looped up from the wells in nylon loops (CrysCap system from Hampton Research), dipped for ~20 s in a cryoprotectant solution, and plunged into liquid nitrogen. Crystals were stored under liquid nitrogen in cryovials and transferred to and from the goniometer and cold stream using cryo-tongs from Hampton Research.

Data reduction

Integration of spot intensities from detector images, scaling the individual images, and scaling together different data sets was carried out using Denzo and Scalepack, in the HKL package (Otwinowski et al. 2003). The final refinement was carried out with data from a single

frozen monoclinic crystal collected in three datasets. The first was at SSRL beamline 7.1, wavelength 1.08 Å, with the Mar345 IP at 400 mm, scanning a 30 cm diameter image. In this run 205 1° images were collected and processed to 3.3 Å. The second dataset was at the ALS beamline 5.0.2, wavelength 1.1 Å, using the ADSC Q4 detector at 240 mm. There 180 images (1°) were collected and again processed to 3.3 Å. Finally a low resolution dataset was collected under the same conditions as the second but with a short exposure time (10 s) to avoid saturating strong low-resolution spots, and processed to 3.8 Å.

Integration of each dataset was repeated several times with different parameters. Scalepack found the mosaicity to be 1.74°. When the data was integrated assuming a slightly higher mosaicity to ensure that overlapped spots were rejected and that all contributing frames were included in measuring each reflection, fairly accurate data could be obtained- R-sym(I) of 5.9% to 3.3 Å and 35% in the shell at 3.5 Å. However this resulted in most of the spots being rejected as overlapped, so the completeness was only 45% to 3.3 Å and 37% at 3.5 Å.

In order to improve completeness at the expense of accuracy, the integration was repeated assuming smaller values of mosaicity and with different integration box parameters. Assuming 1° mosaicity allowed us to obtain (from 180° of data) 88% completeness to 3.3 Å and 86% completeness in the shell at 3.75 Å; while the R-sym deteriorated to 10% overall and 32% at 3.75 Å. This increase in R-sym overestimates the error introduced: part of the increase results from increased redundancy since the Rsym statistic badly underestimates variability at low redundancy (Diederichs and Karplus 1997).

In the end all of the different runs from the three datasets were merged together to give a dataset with good completeness (96.8% to 3.3 Å) including accurate measurements of those reflections that were observed without overlap averaged together with less accurate estimates of all reflections. When all the integration runs of each dataset were merged separately and then the three datasets were merged together, R-merge values for the latter operation were 9.6% overall and 38.2% at 3.3 Å, suggesting useful data extends to that resolution. However the data is highly anisotropic as indicated by the "fall-off analysis" implemented in the "truncate" program of the CCP4 package (COLLABORATIVE COMPUTATIONAL PROJECT 1994) and by the anisotropic

B-factor tensor refined in CNS which has diagonal elements of 38, -89, and 51 Å². Cell parameters, data reduction statistics, and data refinement statistics are presented in Table 1.

Structure determination

The three crystal forms were solved with ~7.0 Å data by molecular replacement using a 3-subunit cyt *bc*₁ abstracted from chicken cyt *bc*₁ structure 1BCC. The Program AMoRe (Navaza 1994) as presented in the CCP4 package was used for the calculations. In anticipation of the possibility that the same dimeric relation observed in eukaryotic cyt *bc*₁ would exist in the bacterial complex, a dimeric search model was used and the data of the trigonal and tetragonal crystals was expanded to lower point group symmetry (P3 and P4). This strategy, which allows the search model to match a larger fraction of the contents of the unit cell and so give a stronger peak in the rotation function provided that the same dimeric relation exists in the target cell, was successful. The translation function identified the enantiomorph of the trigonal crystal (P3₁12 not P3₂12) and confirmed the symmetry of the tetragonal crystal (P4₂2₁2). Both of these form have a monomer in the asymmetric unit, with the dimer 2-fold axis coinciding with a crystallographic 2-fold axis. The monoclinic crystals (P2₁) which have no crystallographic 2-fold axis, have a dimer in the asymmetric unit. The space group, cell parameters, asymmetric unit content and solvent content for the three crystal forms are summarized in Table 1.

The molecular replacement solutions were refined by rigid body and domain rigid body refinement and used to phase the data. The initial phases were improved and model bias reduced by multi-crystal-/ncs-averaging and solvent flattening to produce a low-resolution (6.5 Å) density map of the complex (Figure 5). Some limited rebuilding was done in these maps, but the quality and resolution were too low for substantial improvement. Later when some crystals diffracting to higher resolution were produced as described above, several datasets were collected to 3.3 Å, with useful data extending at least to 3.5 Å. Various maps for rebuilding were calculated using the new data by phase extension from the low resolution or new molecular replacement and NCS-averaging, and some significant rebuilding has been carried out in these maps using the program "O" (Jones et al. 1991). In order to combine data from multiple crystals

and combat model bias, most of the rebuilding was done in averaged maps from four of the best monoclinic crystals after many cycles of density modification by multi-crystal+NCS averaging and solvent flattening; each crystal being initially phased with the model from the previous cycle refined against the data of that crystal. Multicrystal averaging was carried out with the Rave (Kleywegt and Jones 1994) and CCP4 packages, calculating 2Fo-Fc maps from each crystal at the start of each cycle, using the "Fill-in" option of CCP4 "sfall" so that missing data would not distort the maps. The averaged map from the final cycle was used for rebuilding the model. The general correctness of the solution is confirmed by (1) strong peaks at the Iron positions in anomalous difference maps with the density modified phases, and (2) appearance in the averaging map of large features intentionally omitted from the model as a test during the previous refinement and phasing. In efforts to get experimental phases, 12 datasets of crystals soaked with five different heavy-atom reagents have been analyzed by difference Fourier methods, but no heavy atom sites were found. Using multi-wavelength anomalous data the positions of Fe atoms can be stably refined, however the phasing power from the anomalous signal is negligible.

Refinement was carried out with the CNS program package (Brunger et al. 1998), using single rigid body rotation, domain rigid body rotation, positional refinement, and restrained atomic B-factor refinement. Strong NCS restraints were used during the positional refinement, and later when it was clear that many regions had the same structure as the bovine protein the secondary structure was enforced in those regions by "patching" hydrogen bonds based on the bovine structure. The progress of refinement was followed by the crystallographic R-factor, and the appropriateness of refinement protocols was judged by cross-validation and the Free-R factor (Brunger 1992). The best diffraction dataset described above, and the atomic coordinates of the current best model refined against that dataset, have been deposited with the Protein Data Bank as entry 1xxx.

Due to the small number of data the refinement problem is not very well determined and the gap between the crystallographic R and the R-free factor is large (~6%), and model bias is a real problem during rebuilding. It must be emphasized that this is not a highly refined structure that

satisfactorily accounts for all the data, but rather a preliminary structure that we hope to further improve in the future either by obtaining better crystals or by the gradual bootstrap process of correctly rebuilding a few features in the current ambiguous density to get better phases, giving better maps on the next cycle which allow further corrections, and so on.

Results and Discussion

The overall structure of *Rb. capsulatus* cyt *bc*₁

Similar to the mitochondrial and chloroplast enzymes, *Rb. capsulatus* cyt *bc*₁ structure is also an intertwined homodimer with the two monomers organized around a twofold molecular axis. Of the three catalytic subunits, the membrane extrinsic domain of the FeS protein is together with the cyt *b* and cyt *c*₁ subunits on the one monomer, while its membrane anchor is assembled with the same subunits on the other monomer. Bacterial cyt *bc*₁ is smaller (a total of 886 amino acid residues in *Rb. capsulatus*) than the mitochondrial cyt *bc*₁ (2166 amino acid residues in beef (Schagger et al. 1995) or 2079 in *Saccharomyces cerevisiae*) (Zhang et al. 1998) or even the chloroplast cyt *b*₆*f* (975 amino acid residues in *Chlamydomonas reinhardtii*) ((Kurusu et al. 2003; Stroebel et al. 2003). These cyt *bc* complexes contain eight, seven and four additional non-catalytic subunits, respectively (Figure 1).

The number of the trans membrane helices that form the central core of the enzyme is the smallest in the case of the bacterial cyt *bc*₁ (a total of ten with eight from cyt *b*, one from the FeS protein and one from cyt *c*₁, versus 13 in the mitochondrial cyt *bc*₁ or chloroplast cyt *b*₆*f*). Remarkably though, with the exception of cyt *b* helix H, which is absent in the cyt *b*₆*f*, overall positions in respect to each other of the ten helices from the catalytic subunits are conserved in all cases. The massive core proteins, extruding into the aqueous phase on the N side of the membrane are unique to the mitochondrial enzyme, and both the structure and the position of the heme group of cyt *f* are not comparable to its counterpart in the other complexes ((Zhang et al. 1998; Stroebel et al. 2003). Otherwise, the overall shape of the catalytic subunits and the relative positions of their redox cofactors are highly conserved and the secondary structural elements are very similar between the three classes of *bc/bf* complexes. Major structural differences are due to changes in the position, length and conformation of several connecting loops due to species-specific insertions and

deletions, as described below.

***Rb. capsulatus* cyt *bc*₁ versus its mitochondrial and chloroplast homologues**

Cyt *b* subunit: Cyt *b* has been a favorite tool of molecular evolutionists who have accumulated for comparison purposes a large number of primary sequences for this protein from a variety of organisms (Degli Esposti et al. 1993). Their comparison indicates that the bacterial cyt *b* is about fifty residues longer than its mitochondrial and chloroplast (cyt *b*₆ and subunit IV together) counterparts. In the case of *Rb. capsulatus* it has 437 residues as compared to 379, 380, and 385 for cow, chicken, and baker's yeast proteins, respectively. Like its mitochondrial and chloroplast homologues, the first four helices of the bacterial cyt *b* (Helix A (residue 46 to 67); B (89 to 118), C (125 to 148) and D (188 to 219)) form a transmembrane four-helix bundle that entraps the two *b*-type hemes (*b*_L for low potential and *b*_H for high potential *b*-type heme), one near each end. These hemes are axially coordinated between the histidines 97 and 111 of helix B and 198 and 212 of helix D, respectively (Yun et al. 1991), with the individual protoporphyrin planes being parallel to the axis of the 4-helix bundle but rotated about that axis by an angle of about 50°, one relative to the other. The heme propionates on the D rings of the hemes are directed outward toward the membrane surface on either side, with the vinyl groups on the B rings directed inwardly, facing each other across a gap of 7.5 Å.

The remaining four helices (helix E to H) are devoid of any prosthetic group, and helix E (residue 243 to 270), which is in close proximity to that of the FeS protein subunit of the opposite monomer, runs in an anti parallel orientation to the trans membrane helical anchor of cyt *c*₁. Several α -helical surface domains such as *ab*, *cd1* and *cd2* on the periplasmic and helix α -*a* on the cytoplasmic side of the membrane are also quite similar in the mitochondrial and bacterial proteins. Lower case letters are used to designate non-transmembrane helices as distinct from the eight transmembrane helices A through H. Helix

α -a is located before transmembrane helix A in the sequence, while *ab* and the two *cd* helices are located between transmembrane helices A and B and between C and D, respectively.

The fifty or so additional residues of the bacterial *cyt b* are distributed between the N- and C- termini and three internal insertions (Figure 2, regions numbered 1 to 5), of which one is shared with yeast protein. As noted in comparing the mitochondrial and chloroplast *cyts* (Soriano et al. 1999), the changes are concentrated on the "N" side of the protein, while the P side is highly conserved. Since the electron transfer functions of the bacterial and mitochondrial complexes appear to be identical, the differences are likely to be related to the presence or absence of the supernumerary subunits 1, 2, and 6 which dominate the N-side surface in the mitochondrial complex.

Omitting these five regions to be discussed in detail below, the remaining 344 residues of *Rb. capsulatus* *cyt b* encompassing amino acids 40-122, 125-227, 241-309, and 329-417 could be superimposed with the corresponding residues from the bovine structure 1PPJ ((Berry et al. 2003)) with a root mean square positional deviation (RMSD) of 1.02 Å. Moreover, when the same residues in both monomers of the dimeric structure are superimposed between these two structures, the RMSD for the 688 residues is not significantly higher (1.17 Å), implying that the structural relationship between the two monomers is essentially the same in the bacterial and mitochondrial *cyt b*. Because *cyt b* serves as the central core of the complex onto which other subunits are bound, the alignment of the above-indicated residues in the *cyt b* dimer was used to superimpose the structures of various *cyt bc₁* and *cyt b_{6f}* complexes in order to compare the relative location of their other features. As the non crystallographic symmetry was strongly restrained during refinement to improve the data + constraints / parameters ratio, it is not surprising that these residues superimpose well (RMSD of 0.025 Å) between the two monomers in the *Rb. capsulatus* structure. Furthermore, the same operator can simultaneously superimpose the dimer onto itself, with RMSD of 0.072 Å. As this feature was not constrained during

refinement, this implies that the proper two-fold symmetry of the basic fold is not distorted by crystal packing.

Region 1: N-terminal differences. *Rb. capsulatus* cyt *b* has 15, 14, 13 and 12 extra N-terminal residues as compared with yeast, cow, chicken and *C. reinhardtii* proteins, respectively. Working from the beginning of transmembrane helix A back toward the N-terminus, the bacterial cyt has strong density consistent with a structure similar to that of the yeast or chicken cyts (1P84 and 3BCC) as far as those structures go. Ironically the high-resolution bovine structure 1PPJ is poorly ordered in this region, so the best comparison is with the yeast structure. The amphipathic surface helix α -a, made up of residues 23 to 34, is superimposable with that of yeast or chicken. This helix runs parallel to the surface of the membrane going toward the other monomer of cyt *b* to make a dimer contact, with Pro23 closely approaching Trp214 near the end of helix D of the other cyt *b* monomer.

The last turn of helix α -a (which consists of a π -bulge in the chicken and yeast structures) makes part of the wall of the Q_i site. This is seen also in the bacterial structure, with a possible H-bond between the carbonyl of Asp31 with Ne2 of the quinone-liganding His217. The dimer contact at the beginning of helix α -a mentioned above also seems to be a conserved feature, although the specific residues involved are not. The α -a helix can thus be seen as a rod connecting the Q_i site and specifically His217 in one monomer with the end of the D2 helix around 214 in the other monomer, and so might allow communication between the Q_i sites. This would be consistent with the sometimes poor order and indications of multiple conformations that exist in the current structures. However there is no evidence yet to support this highly speculative suggestion. A more likely role for the α -a helix is to prop apart the N-side end of the dimeric cyt *b* to optimize the geometry of the lipid-filled clefts for quinone diffusion between the active sites.

Before the dimer contact, the structures diverge. There is a right angle turn at the dimer contact preceded by a short helical stretch (residues 3 to 7 in yeast). In the

mitochondrial cyt a pair of conserved basic residues in this helical stretch, Arg4 and Lys5 in yeast, interact with residues in subunit 1 of the same monomer. These residues are not conserved in the bacterial cyts, which have no counterpart corresponding to subunit 1. In *Rb. capsulatus* the helical segment is longer, running from about 14 to 21, and displaced from the corresponding segment of yeast. Before this the density extends in a thin strand back to a starting point near the linker between helices D and E (of the same monomer), which we have modeled as extended coil comprising residues 2 to 13. Individual residues cannot be made out in this density, so the assignment is somewhat tenuous.

Region 2: The first internal insert of the bacterial cyt *b* corresponds to residues 123-124, and should rather be called a deletion of the vertebrate mitochondrial cyt *b* as this region is well conserved in the case of most cyts *b* or *b₆* from bacteria, archaeobacteria, chloroplasts, or from protozoan, algal, plant, or fungal mitochondria (Figure 2c, region 2). This conserved region is the linker between helices B and C and has the consensus motif ₁₂₁YxxPRE. the final E is not conserved in fungi and some archaeobacterial cyts, and the initial Y is replaced by F in cyt *b₆*. In vertebrates and other eumetazoa, the initial Y is present but the conserved Pro124 and the residue preceding it are deleted, and the final Glu is not conserved. The dipeptide which is deleted in vertebrates is indicated in the bacterial, yeast and *b_{6f}* cyts in Figure 2a (red color at position 2).

Based on bovine and yeast structures as well as the current bacterial one, the Tyr124 (106, yeast) makes an H-bond with an aspartate or histidine at residue 350 (309, yeast), holding together the N-side ends of the B, C and F helices. From high-resolution structures of yeast cyt *b*, we also know that the conserved proline (Pro109) forms a *cis*-peptide linkage with the previous residue (Hunte et al. 2000). It is the last non-helical residue before the transmembrane helix C, and may function to "cap" extension of the C helix further N-terminally during its initial folding. A recent high-resolution structure of the bovine enzyme shows similar *cis*-prolines at the beginning of the transmembrane helices D (Pro222) and H (Pro346) (Berry et al. 2003). The Pro222 is not conserved in yeast, although it is present in

other fungi. Interestingly, a revertant of a yeast mutant gained a proline at this position to overcome the need for the core protein 2 of the cyt *bc₁* (di Rago et al. 1997). All three prolines (residues 124, 246, and 388) are present and well-ordered in the *Rb. capsulatus* structure, and the electron density is compatible with them forming *cis*-peptide linkages, although at this resolution a rigorous assignment is not possible.

Region 3: The second insert in *Rb. capsulatus* cyt *b* extends from residues 230 to 237 in the *de* linker near the Q_i site, and is located between positions 214 and 215 of the yeast sequence (Figure 2, region 3). In this region, the *Rb. capsulatus* structure superimposes well with the yeast or bovine structure through residue 227 (corresponding to position 212 in yeast), and again starting with residue 241 (corresponding to position 218 in yeast). The five-residues long linker in the mitochondrial cyt *b* (positions 213 to 217 in yeast) is replaced in the bacterial counterpart by 13 residues (positions 228 to 240 in *Rb. capsulatus*) of which several are positively or negatively charged. Remarkably, this longer bacterial linker encircles subunit 7 of the superimposed bovine or yeast cyt *bc₁*, suggesting that shortening of the mitochondrial linker was required to accommodate the presence of subunit 7, which is absent in the bacterial cyt *bc₁*. This linker is even longer in some other bacterial species (e.g., by five residues in *Chromatium vinosum*). This is in the region where cyt *b₆* and subunit IV of the cyt *b_{6f}* are split to form two distinct polypeptides. If the C-terminus of cyt *b₆* from spinach or *C. reinhardtii* is joined to the N-terminus of subunit IV, and the resulting sequence aligned with cyt *b* from bacteria and mitochondria, the ensuing loop is eight residues longer than that in bacteria. Superimposing the structures of cyt *b_{6f}* and *Rb. capsulatus* cyt *bc₁* (not shown) reveals that the C-terminus of cyt *b₆* diverges only slightly toward its end from the mitochondrial or bacterial cyt *b*, with the terminal C- α atom of residue 215 being less than 3 Å away from residue 210 of yeast or 225 of *Rb. capsulatus*. The N-terminal 27 residues of subunit IV make a loop in the same general region as the loop seen in the bacterial cyt *b*, but with a 10-residue α -helix that is not present in the bacterial structure. Starting with residue 25 the superposition is excellent with yeast mitochondrial or

bacterial cyt *b*. This is partly due to 3 conserved β -bridges stitching together the loops preceding helices A and D. This bridge immobilizes a strand consisting of 218-221 in the yeast, 242-245 in the bacterial, or 24-27 in the subunit IV of the cyt *b_{6f}* sequences. The high degree of structural conservation surrounding the internal insert in region 3 of cyt *b* explains *a posteriori* why the earlier experiments aiming at splitting of a bacterial cyt *b* into two polypeptides were successful both using *Rb. capsulatus* (Saribas et al. 1999) or *Rb. sphaeroides* cyt *bc₁* (Kuras et al. 1998).

Region 4: The only major change on the P side of cyt *b* is an insertion spanning from the residues 308 to 325 of *Rb. capsulatus* cyt *b*, located between the *ef* amphipathic helix and the trans membrane helix F (Figure 2, region 4). The bacterial and mitochondrial structures superimpose well through residue 309 (corresponding to bovine 285) and again starting with residue 328 (corresponding to 286 bovine). However, the residues 309 and 328 are a little farther apart than the corresponding mitochondrial residues, and there is no density connecting them. Instead, each is connected to a nearby cylindrical density of approximately the right length to accommodate the additional residues in a 3-turn α -helix. This insert is poorly defined in the density, so the details should not be taken too seriously until a better refinement is achieved. Mitochondrial residues 285 and 286 form part of the rim of the docking "crater" for the FeS protein, and are in van der Waals contact with Pro175 (bacterial Pro170) in the third loop of the head domain of the latter subunit when it is located in the cyt *b* position. The insert in the bacterial protein opens a gap that could facilitate movement in and out of the crater.

Region 5: (Figure 2, region 5). The last transmembrane helix, G, is missing altogether in the cyt *b_{6f}* and of variable length in the mitochondrial cyt *bc₁*. In those structures available it extends nearly to the C-terminus, so that the two or three residues following the last helix make no significant contacts and don't seem to play any role. The helix is longer by six residues in the yeast protein compared to bovine, while cyt *b* of *Toxoplasma gondii* is truncated (McFadden et al. 2000) at the level of bovine residue 369, 8

residues before the end of the helix.

Although the C-terminus of *Rb. capsulatus* is extended by 16 amino acids compared to the vertebrate, helix H ends early compared to its yeast or even bovine counterparts. The last residue in this helix is Lys416, perhaps because the helix is capped by Pro417, which corresponds to 376 in the yeast or chicken sequence, and is conserved in proteobacteria. In *Rb. capsulatus* cyt *b* the extra C-terminal residues plus the shorter helix result in a 20-residue extended coil from position 417 to the end, initially passing over the end of helix G making β -bridges (between residues 360 and 418) that holding together the N-side ends of helices G and H. In the mitochondrial complex subunit 6 surrounds helix H, perhaps compensating for the lack of this connection.

Quinone binding sites. There is density for a quinone at the Q_i site in the same position as in the yeast or chicken structures (1ezv or 2bcc), however with the current resolution and state of refinement the orientation of the ring is not defined. The quinone-liganding His217 is in the same position as the corresponding residue in the chicken or cow structures, different from that seen in yeast. We think both positions may be correct and that movement of this residue may occur during the catalytic cycle.

The true physical location and the exact number of Q/QH₂ molecules at the Q_o site are currently uncertain due to absence of such molecule(s) in this region or highly disordered state of the quinone (e.g. 1NTZ) in the available structures. In the present structure the Q_o site is occupied by stigmatellin which seems to facilitate crystallization in this space group, perhaps by fixing the position of the ISP which is involved in some of the crystals contacts. The same crystal form has been obtained without stigmatellin, however the resolution (7 Å) was not high enough to describe the occupation of the Q_o site. Efforts are currently under way to crystallize one of the "neck" mutants (Darrouzet et al. 2000; Cooley et al. 2004), which seem to hold the ISP preferentially in a position similar to the stigmatellin position, in the absence of stigmatellin.

Cyt c_1 and cyt f subunits: Mitochondrial and bacterial cyts c_1 are class I c-type cyts while cyt f is unique:

Among the proteobacterial and mitochondrial complexes, the cyt c subunits are clearly closely related based on sequence, and so these are all called cyt c_1 after the mitochondrial example. The first x-ray structure containing a cyt c_1 was the chicken cyt bc_1 (Zhang et al.) and it showed that structurally cyt c_1 was a member of Ambler's class I cyts (Ambler 1982). On the other hand the cyt c subunit of the cyt b_6f complex, cyt f , has little in common with cyt c_1 or any class I cyts.

Both cyt c_1 and cyt f are anchored to the membrane by a C-terminal trans membrane helix, have their N-termini located on the P side of the membrane, and their membrane-extrinsic domains house a c-type heme that is reduced by a [2Fe2S] cluster. Yet cyt f appears to be completely unrelated to cyt c_1 with respect to their protein folds (Figure 3). These two proteins interact physically with very different electron acceptors: a c-type cyt (cyt c , c_2 , c_7 or c_8) (Jenney et al. 1994; Kerfeld et al. 1996) or a high potential iron-sulfur protein (HiPIP) (Hochkoeppler et al. 1996) in the case of the cyt c_1 versus plastocyanin or a c-type cyt (cyt c_6) in the case of the cyt f (Cramer et al. 1996). Moreover, the pH of the environment in which these subunits perform their specific functions is very different between the bacteria, mitochondria and chloroplasts. In addition, the positions of the heme domains, in particular the distances between the heme-irons of each monomer and the orientations of the cyt c_1 and cyt f heme planes are also dissimilar, with the former being almost perpendicular to the membrane, and the latter at a 25-30° angle from it ((Kurusu et al. 2003; Stroebel et al. 2003)). Finally, although one axial ligand of the heme is His in both cyts, the other axial ligand is Met in cyt c_1 while the NH₂ group of the N-terminus plays this role in cyt f ((Martinez et al. 1994)).

As in the mitochondrial enzyme the membrane extrinsic domain of bacterial cyt c_1

sits atop the A, B, C, D helices and their connecting loops of cyt *b*, while its membrane anchor runs parallel to the α -helix E of cyt *b* (Iwata et al. 1998; Zhang et al. 1998; Hunte et al. 2000). Even between the closely related proteobacterial and mitochondrial cyt *c*₁ there are major differences that will be discussed below.

The mitochondrial cyt *c*₁ as seen in the structures of the eukaryotic cyt *bc*₁ (Iwata et al. 1998; Zhang et al. 1998; Hunte et al. 2000), has a core folding pattern similar to that of the class I *c*-type cyts although it also exhibits major differences in the inter-helical domains. The core of the class I *c*-type cyts consists of the helix α -1 bearing the "heme fingerprint" CxxCH sequence at its end, the highly conserved heme-supporting stretch with its conserved P(N,D)L(x)₆R sequence, and the helices α -3 and α -5 (Figure 3). This core structure is quite similar between the bacterial and mitochondrial cyts *c*₁, as a structure-based alignment of these sections (*Rb. capsulatus* residues 20-38, 97-107, 126-134 and 182-222 aligned to bovine residues 23-41, 110-120, 122-130 and 158-198, respectively) reveal no insertions or deletions between them, and the C- α atoms are accurately superimposable (see below). On the other hand, among various species, significant insertions and deletions are seen mainly in the interhelical regions of low homology.

The helix α -4 of class I *c*-type cyts is missing in cyt *c*₁ and is replaced by a binding site for the "hinge protein", and the helix α -2 together with a long loop that covers the propionate-bearing edge of the heme (rings A and D of the tetrapyrrole moiety) are also absent (Figure 3, left). The latter feature is characteristic of the so-called "small" class I *c*-type cyts such as cyt *c*₅₅₁ of *Pseudomonas aeruginosa*, ironically making the otherwise quite large cyt *c*₁ a member of this subclass. More importantly, exposure of the heme propionate edge allows close proximity of the FeS protein on this side (Zhang et al. 1998), opening up a "back-door" electron donation access to the heme, in addition to the traditional exposure of the C ring on the other side of the protein. Comparing Cyt *bc*₁ structures such as 1BCC (Zhang et al. 1998) and 1BE3 (Iwata et al. 1998) with the FeS protein head domain in cyt *c*₁ position, and 1KYO (Lange and Hunte 2002) with cyt *c* bound to cyt *c*₁ indicate that both the

electron donor and acceptor partners can be bound simultaneously to cyt c_1 with reduction and oxidation taking place by separate pathways. This is in contrast with other redox proteins such as cyt c or the FeS protein, which when interfaced with one redox partner are excluded from interacting with another.

In the case of the cyt b_6f , as the available structures have the FeS protein head domain in or near the cyt b position (Kurisu et al. 2003; Stroebel et al. 2003), it is not yet clear how the electron donor interacts with cyt f . It has been proposed (Kurisu et al. 2003) that movement of the FeS protein toward cyt f would place the [2Fe2S] cluster near residue Leu27 of the cyt subunit. A docking site for plastocyanin on soluble cyt f has been refined against NMR distance restraints ((Crowley et al. 2002)), and this model puts plastocyanin near the exposed heme propionates on the other side of cyt f in respect to the FeS protein. Thus, it is likely that in cyt b_6f also separate pathways exist for electron transfer with reductant and oxidant, allowing simultaneous interaction of both the FeS protein and plastocyanin with cyt f . However, it is noteworthy that in the case of cyt f , contrary to cyt c_1 , the heme propionates are directed toward the physiological electron acceptor plastocyanin while the C corner of the heme is exposed on the side facing the FeS protein.

Otherwise the cyt c_1 and cyt f are poorly comparable, hence the discussion will focus on differences between mitochondrial and bacterial cyts c_1 . Sequence alignment of these cyts c_1 shows significant insertions and deletions in various species, again mainly in the interhelical regions. Where the inserts occur in regions of low homology, the alignment based on sequence alone can be somewhat arbitrary. Now that a structure is available, a structure-based alignment can be obtained (Figure 3c), in which insertions and deletions are adjusted to align residues that are close together in the superimposed structures.

Helix α -1 and heme binding fingerprint region: Cyt c_1 is anchored to the membrane with a C-terminal trans membrane helix, and in the mitochondrial or bacterial cyt bc_1 it is the only transmembranous subunit with its N-terminus located on the P side of the membrane. In *Rb. capsulatus* cyt c_1 the first helix of the membrane extrinsic domain, helix α -1, starts

with residue 20 corresponding to residue 23 of the bovine sequence. Before this helix, cyt c_1 polypeptide chain is extended with little secondary structure, and in the mitochondrial enzyme it contacts the acidic “hinge” protein. In this respect it is noteworthy that *P. denitrificans* cyt c_1 has a long acidic insert in this region, which was suggested early on as a possible substitute for, or precursor of, the hinge protein (Kurowski and Ludwig 1987). Next, in both the mitochondrial and bacterial cyts c_1 the chain dips down into the membrane just before entering helix α -1 (Figure 3). In *Rb. capsulatus* cyt c_1 this feature consists of the highly conserved Gly13 and the adjacent hydrophobic residues Ile and Phe at positions 14 and 15. This loop may serve as a “second anchor” to stabilize the position of the globular extrinsic domain of cyt c_1 (Berry et al. 1999), as these residues (Leu17 and Leu18 in bovine and Ile14 and Phe15 in *Rb. capsulatus*) have their side chains directed down into the membrane at the edge of the helical platform, with residue 17 in van der Waals contact with the aromatic ring of the conserved Tyr269 (corresponding to Phe245 in the bovine sequence) in helix E of cyt b (Figure 3b).

In all class I c -type cyts, helix α -1 and the heme-binding fingerprint region contains a highly conserved pair of arginines (e.g., Arg24 and 25 in *Rb. capsulatus*). In the bovine structure the first arginine interacts with a glutamate in the first branch of the branched loop (see below) and with Asp172 (Asp196 in *Rb. capsulatus*) at the tip of the loop between the Met ligand and helix α -5. The second arginine ion pairs with a glutamate in helix α -5, which crosses helix α -1 at the conserved Gly26. Tyr30 is an aromatic residue which is co-conserved with Phe213 in helix α -5 in all class I c -type cyts, where one of the residues is always a Phe while the other is always a Tyr, and *vice versa*. These residues make a distant van der Waals contact without involving the hydroxyl group or the C α atoms, hence the reason for their high co-conservation is not obvious.

Heme-stabilizing stretch PDL(x)₆R region: Another highly conserved feature of class I c -type cyts is a motif P[N,D]L(x)₅₋₆[K,R], corresponding to ₉₈PDLSVMAKAR₁₀₇ in *Rb. capsulatus*. The carbonyl oxygen of Pro98 accepts a hydrogen bond from the heme fifth

ligand His38. The second residue of the motif (Asp in cyts c_1 but Asn in cyt c or c_2) faces away from the heme, and H-bonds with main-chain atoms in the stretch following the heme fingerprint region and in the heme-stabilizing stretch (K41n and S101 in *Rb. capsulatus*) holding these disparate regions together (Figure 3). The third residue of the motif, Leu100 in *Rb. capsulatus* faces toward the heme, contributing to the hydrophobic nature of the heme pocket and making van der Waals contact with the imidazole ring of heme ligand His38. At the other end of the conserved stretch Arg107 ion-pairs with the propionate from the A ring of the heme tetrapyrrole. In cyts c and c_2 there are only five residues between the PNL triplet and the conserved Arg.

Sixth axial ligand Met and helix α -5 region: The C-terminal portion of *Rb. capsulatus* cyt c_1 from the sixth axial ligand Met183 through the helix α -5 and the trans membrane anchor helix aligns well with its mitochondrial counterparts, and superimposes well with the bovine structure (Figure 3A, middle and right), although its C-terminus is shorter by six residues, due to the absence of the last amino acids which are involved in a β -sheet with subunits 1 and 7 in the mitochondrial cyt bc_1 . The C- α atoms of residues 182 to 256 superimpose on the bovine residues 158 to 232 with an RMSD of 1.24 Å. This deviation is partly due to the angle between the extrinsic domain and the transmembrane helix in the two cyts c_1 differing by 5 degrees. Superimposing the conserved parts excluding the transmembrane helix, that is superimposing helix α -1, the heme-supporting stretch 98-107, α -3, and from the Met ligand through the end of helix α -5, gives RMSD of 0.88 Å.

Outside of the highly conserved core region described above, typical features that characterize the mitochondrial cyt c_1 and additional differences revealed by the new *Rb. capsulatus* structure are as follows.

The branched loop and helix α -2' reveal no dimer interface in *Rb. capsulatus* cyt bc_1 ; The loop between the heme fingerprint region at the end of helix α -1 and the heme-bracing triplet PDL is highly variable in class I c -type cyts. In the case of the mitochondrial

cyt c_1 this consists of a long branched loop and a new helix α -2' (Figure 3). The first fork of the branched loop folds back against helix α -1 and includes conserved acidic residues considered to be important for cyt c docking (Stonehuerner et al. 1985). The second fork of the branched loop and the new helix α -2' form the two surfaces of a dimer contact with cyt c_1 in the other monomer. The forked loop is similar in *Rb. capsulatus* cyt c_1 as expected from the fairly good sequence conservation between residues 37-92 (*Rb. capsulatus* numbering). Its first fork, consisting of residues 46 to 61, is longer than the bovine counterpart due to insertion of residues on either side of conserved Gly52 in the turn. Nonetheless, conserved residues play a similar role in the mitochondrial and bacterial enzyme. Arg46 of cyt c_1 makes a two-bonded ion pair with Asp86 in cyt b , and the resulting locked side chains provide a strap supporting one side of the hinge of the FeS protein (residues Ser41 and Ala42) where it emerges from the cyt b dimer.

In *Rb. capsulatus* cyt c_1 an α helix starting with residue 58 in the returning strand of the first fork continues until residue 66 in the second fork, and a Phe is found in the quasi-completely conserved [E/Q] position 60, which in the bovine cyt c_1 interacts with a conserved Arg (corresponding to Arg24 in *Rb. capsulatus*) in helix α -1. No electron density for the side chain of Arg42 is observed in the present density map, suggesting that it may be disordered in the absence of its ion-pairing partner Glu60 in the mitochondrial cyt c_1 . The rest of the second fork is a β -hairpin, with a reverse turn including the conserved Gly77, and is three residues shorter than its mitochondrial counterpart. It lacks the *cis*-peptide associated with Pro74 in the bovine enzyme which distorts this β -hairpin in the latter case. While the current resolution of *Rb. capsulatus* data does not allow as yet building of an atomically correct model, still the density map is consistent with a gently curved hairpin structure in this region. Finally, bacterial residues 80 to 92 superimpose fairly well with residues 83 to 95 of the bovine cyt c_1 , constituting the returning strand of the branched loop. As in the bovine structure, the density map provides evidence for interaction of conserved Arg80 with Asp86 and Asp73. Bacterial cyts c_1 contain a deletion of 11 residues relative to the bovine

counterpart between the branched loop and the heme-bracing triplet $_{98}\text{PDL}$, thus eliminating helix $\alpha\text{-2}'$ involved in the dimer contact. In the mitochondrial cyt c_1 the tip of the second fork of the branched loop in each monomer contacts helix $\alpha\text{-2}'$ in the other monomer. As a result of the shorter second branch and the missing helix $\alpha\text{-2}'$ region in *Rb. capsulatus* cyt c_1 , there is no contact between the two cyt c_1 molecules in the bacterial cyt bc_1 dimer.

The loop before helix $\alpha\text{-3}$ does not cover the heme propionates: In "large" class I c -type cyts such as cyts c and c_2 , the heme propionates are covered by helix $\alpha\text{-2}$ and the long loop connecting the conserved heme-supporting stretch to helix $\alpha\text{-2}$ (Figure 3 left, colored red in horse cyt c). Both the loop and helix $\alpha\text{-2}$ are replaced by a direct connection of only two residues in mitochondrial and most bacterial cyts c_1 (Figure 3, central model). However, *Rhodobacteriaceae* (*Rhodobacter* and *Paracoccus*) and *Rhizobiales* (*Bradyrhizobium* and *Blastochloris*) cyt c_1 have an insert nearly as long as that found in cyts c or c_2 , suggesting that the propionate edge of the heme may not be exposed in these species. Thus, it is interesting to track down the folding of this part of *Rb. capsulatus* cyt c_1 structure. As expected, the electron density shows no indication of the loop covering the heme edge. Instead, a mass of poorly-interpretable density running approximately at the level of the membrane surface on the side of helix $\alpha\text{-3}$, away from the heme cleft, is visible. Although the position of the C- α backbone is by no means well determined, none the less a loop of the right length was traced through this density, just to visualize the general area where the protein seems to be without blocking access to the heme propionate edge (Figure 3, region shown in red). It is tempting to suppose that the situation encountered here represents an intermediate evolutionary state in which the loop covering the heme has been displaced to expose it, but the now superfluous residues making up this loop have not yet been lost. However, since this loop occurs only in some α -*proteobacteriaceae*, this would require invoking either lateral gene transfer or the assumption that this subgroup is ancestral not only to mitochondria but to other divisions of proteobacter and firmicutes, which have the mitochondrial situation.

The "hinge protein"- binding region is linked by a disulfide bond to an extra loop in the "Hinge Protein" position: After helix α -3 in the bovine structure the polypeptide chain loops back and forth between the surface and interior. Two outwardly facing loops around residues 140 and 152 form a binding site for the acidic hinge protein (subunit 8) of mitochondrial cyt *bc*₁. Residue 140 is a conserved glycine in mitochondrial cyt *c*₁ sequences, and the bovine structure shows it to be in van der Waals contact with residue 53 of the hinge protein, just before the beginning of the helix in the second branch of the hairpin which is formed by the ordered part of the hinge protein (Figure 3). The next residue of the hinge protein, Cys54, while being the beginning of the helix is involved in one of two disulfide bonds present between the branches of the hinge protein. The *Rb. capsulatus* cyt *c*₁ sequence is alignable with that of the bovine through most of this hinge protein-binding region, including conserved residues Pro138, Gly146 Asn150 and Phe153 Pro143, Gly152 Asn156 and Phe159. The above-mentioned Gly140 (bovine numbering), which is only conserved in eukaryotes, is replaced by Cys145 in *Rb capsulatus* cyt *c*₁. The density from the bacterial crystals is fairly good through this region, and follows closely the bovine structure as far as residue 160 which aligns with 154 in bovine. At this point the *Rhodobacter* backbone loops out away from the bovine structure, missing bovine residue 155 and returning around residue 156. The electron density is good from bovine residue 156 to the sixth axial ligand, Met160 in bovine and Met184 in *Rb. capsulatus* with bacterial residue Ser180 superimposing with bovine 156. This tracing indicates that bovine residue 155 is replaced by a long loop extending from residue 161 to 179 in *Rb. capsulatus* cyt *c*₁. Although the density for this loop is less good than for the conserved parts, none the less contouring at a low level of confidence allows tracing roughly its path. This loop passes through a blob of strong density connected to the side-chain of the above-mentioned Cys145. This blob can be modeled as a second cystein residue forming a disulfide with Cys145, as proposed earlier (Osyczka et al. 2001), and threading the loop brings Cys168 into this blob within the uncertainty allowed by the weak density. It is noteworthy that *Rb capsulatus* cyt *c*₁ residues 170 to 178 are in the area occupied by the hinge protein in the

mitochondrial cyt *bc*₁. The presence of a unique disulfide bridge between the residues Cys148 and Cys168 anchoring a loop in *Rb. capsulatus* has been proposed based on biochemical and mutational data (Osyczka et al. 2001). Elimination of the disulfide and its absence decreases the E_m dramatically unless a β -branched amino acid is present two residues away from the heme sixth ligand Met, like in the mitochondrial cyt *c*₁. Indeed cyt *c*₁ mutants lacking this disulfide bridge have much lower E_m values (E_{m7} of about -50 mV), unless they acquire a β -branched amino acid residue near the heme macrocycle via an additional mutation. Such double mutants have functional E_m values (E_{m7} around 230 mV) but they exhibit highly pronounced auto oxidation properties similar to that described for the isolated mitochondrial cyt *c*₁ subunits (Osyczka et al. 2001).

Iron-Sulfur (FeS) protein: Like the mitochondrial but with some extra features.

As expected, the overall structure of *Rb. capsulatus* FeS protein is very similar, to its counterparts in its homologous enzymes, with a base fold and a cluster-bearing fold regions formed of the β -sheets 1, 2 and 3 as described in detail earlier (Carrell et al. 1997). Major differences between the bacterial and mitochondrial FeS proteins include a truncated N-terminus, a 3-residue deletion in the trans-membrane helix, and two insertions in the extrinsic domain (Figure 4). In the mitochondrial cyt *bc*₁ the N-terminus of the FeS protein extends well into the "core" proteins domain on the N side of the membrane, making a number of hydrogen bonds that may aid in anchoring the core proteins to the cyt *bc*₁. Since the core proteins are not present in the bacterial cyt *bc*₁, it is not surprising that these N-terminal residues are missing from the bacterial FeS protein. In *Rb. capsulatus* structure the trans membrane helix of the FeS protein starts with residue 11 as residues before this position are not clear enough to model at this time. When the bacterial and mitochondrial cyts *bc*₁ are aligned as described above based on the cyt *b* dimer, the trans membrane helix anchor of the two FeS proteins are significantly displaced one from the other (Figure 4).

Both pass through the membrane at a large angle from vertical, but this tilt is greater in the mitochondrial case.

This seems to be due to an insertion of exactly three residues into the mitochondrial FeS protein which lengthens this helix by one turn while maintaining the same rotational orientation of the two ends. The mitochondrial and proteobacterial transmembrane helices can be aligned using conserved sections at their either ends: On the N-terminal end of the membrane-anchoring helix there is a cluster of basic and aromatic residues, $_{11}R(R/K)xFxY$, starting at position 11 corresponding to the Tat (twin arginine translocation) specific signal sequence, and there is a conserved motif $_{38}MxxSxDV$ towards the flexible hinge region after the C-terminal end of this helix. Aligning these two regions exposes a 3-residue insert in the mitochondrial sequence compared to its proteobacterial counterpart. Assuming the basic/aromatic region locates itself at the N side of the membrane in both *cyt_{b₆f}*, and a similar thickness of the membrane, this implies that the shorter bacterial helix crosses the membrane at a steeper angle, as observed here (Figure 4B). The basic and aromatic amino acid stretch starting at residue 11 makes an amphipathic section which may serve to fix this region at the membrane surface (due to its slant, one side of it faces the aqueous phase and the other faces the membrane) to perhaps prevent rotation of the anchoring helix.

The *cyt_{b₆f}* FeS protein has the conserved pair of basic residues on the N side, but the sequence around the neck region has no significant homology. However X-ray structures of the *cyt_{b₆f}* (Kurisu et al. 2003; Stroebel et al. 2003) support the alignment of Figure 4c, in which Pro70 of *Chl. reinhardtii* and Pro44 of *M. laminosus* align with Ala64 of bovine or Ala40 of *Rb capsulatus* (this residue is proline in other bacterial species). Using this alignment, the *cyt_{b₆f}* FeS transmembrane helix is the same length as the bacterial ones, and the three-residue insert occurs only in the mitochondrial proteins. Again assuming the same thickness of the membrane this would imply a more nearly vertical transit for the *cyt_{b₆f}* FeS protein compared to mitochondrial, and that is observed. This can easily be

measured as the distance between monomers, measured between C- α carbons in the first of the conserved basic pair in each species. This distance is 85.9 Å between residues R32 for bovine, 79.0 Å between residues R11 for *Rb capsulatus*, 73.5 Å between residues K41 for *Chl. reinhardtii*, and 67.5 Å between residues R15 for *M. laminosus*.

After the trans membrane helix, the FeS protein continues through the flexible "tether" region, strand β -1 (in sheet 1), and β -2 and β -3 (in sheet 2). This region is well conserved between mitochondrial and proteobacterial species even though *Bradyrhizobium*, *Blastochloris*, and *Chromatium* proteins have one extra residue in the tether region. In the *Rb capsulatus* structure the conserved Ser41 and Asp43 side chains are H-bonded as in the mitochondrial structures, holding the intervening sequence in a non-helical loop and initiating the 3-10 helix of the linker. Although the order of these two residues is reversed (DAS instead of SAD) in the *Rhizobiales* (*Rhizobium*, *Agrobacterium*, *Blastochloris*, *Bartonella*) and *Chromatiales* (*C. vinosum*), still possibly they provide the same function.

The cyt *b_{6f}* FeS proteins have an insert in the β 1 - β 2 linker which interrupts β 1 after only two residues. The linker between β 2 and β 3, which contacts cyt *b* when docked in the *b* position, is highly conserved; in particular Pro71 is conserved in all the species compared here, while Gly69 in the turn is conserved in mitochondria, proteobacteria and chloroplasts but becomes glutamate in *B. stearrowthermophilus*.

Two additional loops in the "crest" hairpin: Between strand β -3 and β -4 (both in sheet 2), there is a linker of variable length containing, in the mitochondrial and *Rb capsulatus* proteins, a short helix (residues 79 to 87 in *Rb. capsulatus*) and a conserved motif DxxR (residues 110 to 113). In the mitochondrial structure this loop forms a long multicomponent hairpin along the top of the protein, reaching from the back end forward over the cluster-binding fold and back again. If one sees the extrinsic domain as the head of a bird with the [Fe₂S₂] cluster clasped in its beak, this linker forms a "crest" over the top of the head. The turn at the tip of the hairpin is tied to the cluster-binding fold by a largely conserved acid-

base pair (Arg94 and D95 in *Rb capsulatus*), the side-chains of which form H-bonds with the main chain in the cluster-binding fold. It is the absence of this crest structure that gives the chloroplast FeS protein its distinctive bi-lobed appearance, as the crest bridges over the gap between domains (Figure 4A).

The DxxR motif forms a turn of 3-10 helix with salt-bridges and ion bonds to different parts of the globular domain of the FeS protein. In *Rb. capsulatus* residue Asp110 (corresponding to residue 123 in the bovine sequence) ion-pairs with Arg77 (101 in bovine) holding these parts of the structure together. The guanidino group of *Rb. capsulatus* FeS protein Arg113 (126 bovine) has H-bonds to backbone carbonyl oxygens at positions 163 and 175 (168 and 180 in bovine) in the cluster-binding fold, and to the side chain of nearby Gln121 (mitochondrial only). When the extrinsic domains of bovine and *Rb. capsulatus* FeS proteins are superimposed based on the β -sheet residues, the 3-10 helix with the DxxR motif in the two structures superimposes as well. Before this motif there is an 11-residue insert (Figure 4, region 1) that forms a loop diverging from the mitochondrial structure. Specifically residues 96 to 107 loop out from the bovine structure at the position of residue 120 (bovine) and reach towards the "crossover" linker between the cluster-bearing fold and β -9 in sheet 1. Residues 99 and 100 seem to make parallel β -bridges with residues 177 and 178 just before the linker becomes β -9. Thus this insertion may be adding an additional strand to sheet 1, although the exact H-bonding arrangement is unclear at this time.

Aligning the sequences corresponding to this region from various mitochondrial and bacterial *cyt bc₁* (Figure 4c) shows that *Rhodospirillum*, *Bradyrhizobium*, *Blastochloris* and *Rickettsia* proteins lack this insert, having the same number of residues as the mitochondrial FeS protein. *Pc. denitrificans* has an insert the same length as *Rb. capsulatus*, while *Rb. sphaeroides* and the *Rhizobiales* have an insert 1 residue longer. At the other extreme, the *Helicobacter* protein has fewer residues in this linker than its mitochondrial counterparts and lacks the DxxR motif. As mentioned above, *cyt b_{6f}* FeS lacks the entire crest structure. Finally, although the sequence from *Thermus thermophilus* is too dissimilar to be reliably

aligned by sequence alone, its high-resolution structure (1NYK) (Hunsicker-Wang et al. 2003) indicates that this linker is shorter than that in the mitochondrial proteins, and superposing the structures shows nothing in the region around the DxxR 3-10 helix.

Working with *Rb. sphaeroides*, Xiao *et al.* (Xiao et al. 2004) showed that deleting this insert or mutating all of its residues to alanine was detrimental to the function of the cyt *bc₁*. Further narrowing down the critical residues, mutating either Asp104 or Gly106 to Ala had no effect, while mutating both together yielded a non functional cyt *bc₁*. The *Rb. sphaeroides* Gly106 corresponds to Gly105 in *Rb. capsulatus* and is in a turn, but this residue is not highly conserved among other species containing a similar insert. Considering that *R. sphaeroides* Asp104 corresponds roughly to *Rb. capsulatus* Lys103 which makes a H-bond with residue Asn112 (also conserved in *R. sphaeroides*), a likely possibility is that Asp104 may play a similar role in the latter species. It is not obvious why the effect would be seen only in the double mutant, however.

After the conserved 3-10 helix with the ₁₁₀DxxR motif, the *Rb. capsulatus* sequence exhibits a 7-residue insert relative to the mitochondrial sequences (Figure 4, region 2). Based on the alignment used here no other species has such a long insert in this region: most of the bacteria examined have only one or two additional residues compared to the mitochondrial FeS protein. In *Rb. capsulatus* structure this insert forms a loop which reaches out to sheet 1, with the residues 118 and 119 in the turn of the loop interacting with residues 184 and 185 in sheet 1. Thus, in the case of *Rb. capsulatus* the three sheets of the FeS protein are more tightly connected due to these two loops from the central conserved ₁₁₀RxxD region linking sheet 2 to the sheets 3 and 1. Both loops are on the surface of the FeS protein away from cyt *b*, in what would be bulk solvent in the mitochondrial enzyme. They can be seen as the highlighted flaps in the spacefilling model of the FeS protein in Figure 4d. The bovine protein (1RIE) is shown for comparison, with residues 120 and 128 to 129 highlighted, corresponding to the regions replaced by the loops.

Fe-S subunit: the peptide bond between Gly141 and Pro 142 is found in a *cis* conformation

in the spinach *b₆f* complex whereas in the bovine *bc₁* complex is in *trans* conformation (Carrell et al. 1997; Iwata et al. 1998). The significance, if any of this cis/trans configuration is unknown.

The next major difference is seen in the linker between strands β -5 and β -6 where *Rb. capsulatus* FeS protein has one additional residue as compared with the bovine protein. Examination of the superimposed structures indicate that the residue 149 of the bovine sequence is replaced by the residues 143 and 144 in *Rb capsulatus*. This 1-residue insert appears to be specific to *Rhodobacteriaceae*, with most bacteria having the mitochondrial number of residues, but *R. rubrum* and *C. vinosum* have longer inserts (five and nine residues) in this region. After this insert, the bacterial polypeptide chain continues until its C-terminus without any insertion or deletion as compared with the mitochondrial protein to which it superimposes well. The conserved Pro170 fits the density well assuming the normal trans- peptide linkage with the preceding residue, as in most of the mitochondrial eS structures but unlike the *b₆f* one. In fact, the superimposed 112 residues of the bacterial and mitochondrial FeS proteins located between residues 50-95, 111-113, 125-142, 147-191 have C- α RMSD of 1.20 Å, while simultaneously superposing these C- α atoms in both monomers gave a slightly higher RMSD of 1.32 Å. Clearly, the core structure of the FeS protein, including both the base and the cluster binding folds, is well conserved and the extra residues are accommodated in a small number of insertions in linkers between secondary structure elements. As pointed out previously (Hunsicker-Wang et al. 2003), the modified inserts are on the side of the extrinsic domain facing away from the rest of the complex, while the side contacting the complex is highly conserved.

Position of the FeS protein extrinsic domain: The bacterial cyt *bc₁* is obtained in the presence of stigmatellin, thus as expected, its FeS protein is in the cyt *b* position. It is known that in the dimeric bovine structure from orthorhombic crystals in the presence of stigmatellin (1PPJ), the extrinsic domains of the two FeS protein occupy slightly different positions

relative to *cyt b*, due to crystal packing forces (Berry et al. 2003). In other words, in the structure 1PPJ the non-crystallographic symmetry (ncs) operator relating the FeS protein extrinsic domains is slightly different from that relating the *cyt b* monomers. In the present *Rb capsulatus* structure, the ncs operator superimposing FeS protein extrinsic domains is proper, as the same operator superposes the FeS protein C- α chains of both monomers with RMSD of 0.037 Å. Furthermore, this operator is the same as that relating the *cyt b* monomers, as evidenced by nearly identical direction cosines for the operators, and the fact that one operator could simultaneously superimpose the selected C- α chains of *cyt b* and the FeS protein from one monomer to the other, and *vice versa*, with an RMSD of 0.093 Å. This was not enforced during refinement, as separate NCS operators were used for *cyt b* and the FeS extrinsic domain. An implication is that the inherent symmetry of the dimer is not significantly perturbed by the asymmetric crystal contacts in the lattice.

In the chicken *cyt bc₁*, in the presence of stigmatellin (PDB entry 2bcc), there are no crystal contacts involving the FeS protein, and there also the FeS extrinsic domains obey the same proper two-fold ncs as *cyt b*. To compare the FeS position in the bacterial and mitochondrial complexes, we superimposed the *Rb capsulatus* *cyt b* dimer on that of the chicken *cyt bc₁*, using those conserved residues listed previously and pairing the monomers first one way, and then the other. We found that additional small rotations (6.0° and 6.5° with one pairing, or 5.8° and 6.7° with the other) were required to superimpose each FeS extrinsic domain onto the corresponding chicken domain after the *cyt b* dimers had been superimposed. While the small differences observed may reflect subtle effects of packing forces, the basic difference of about 6.2 degrees is probably a real difference in the resting position of the FeS intrinsic domain in the two *cyts bc₁*. Furthermore although the heme iron atoms were all superimposed to within 0.4 Å by either pairing, the FeS cluster iron positions deviated 0.8 to 1.1 Å, indicating a slightly different position for the extrinsic domain even down near the tip which is H-bonded to stigmatellin in the Qo site.

Conclusion:

While the *Rb capsulatus* cyt *bc₁* is clearly related to mitochondrial cyt *bc₁*'s for which the structures are known, it is a much simpler complex, devoid of any protein chain not associated with a redox factor, and those subunits that are conserved show intriguing differences that may be useful in understanding the evolution of this electron transfer membrane protein complex.

Acknowledgements: This work was supported by NIH grants R01DK44842 (to EAB) and GM38237 (FD). Parts of the work were carried out at the Lawrence Berkeley National Lab (operated by the University of California for the DOE, OBER under contract DE-AC03-76SF00098), The advanced light source (supported by the DOE. The Berkeley Center for Structural biology is supported by NIH), and Stanford Synchrotron Radiation Lab (operated by Stanford University on behalf of the U.S. DOE, Office of Basic Energy Sciences. The SSRL Structural Molecular Biology Program is supported by the DOE, Office of Biological and Environmental Research, and by NIH, National Center for Research Resources and NIGMS). We would especially like to acknowledge the help of R. Keith Henderson at the ALS and Aina Cohen and Dan Harrington at SSRL for help with data collection.

References

- Altschul SF, Madden TL, Schaffer AA, Zhang J, Zhang Z, Miller W and Lipman DJ (1997). "Gapped BLAST and PSI-BLAST: a new generation of protein database search programs." *Nucleic Acids Res* **25**: 3389-402.
- Ambler RP (1982). *The Structure and Classification of Cytochrome c. From Cyclotrons to Cytochromes*. N. O. Kaplan and A. Robinson. New York, Academic press: 263-282.
- Berry EA, Guergova-Kuras M, Huang LS and Crofts AR (2000). "Structure and function of cytochrome bc complexes." *Annual Review of Biochemistry* **69**: 1005-1075.
- Berry EA, Huang LS, Cobessi D, Cromartie TH, Crowley P and Pon NG (2003). "Crystallographic studies of inhibitor and substrate binding in the vertebrate cytochrome bc1 complex at up to 2.1 angstrom resolution." *Biophysical Journal* **84**: 150A-150A.
- Berry EA, Huang LS and DeRose VJ (1991). "Ubiquinol-cytochrome c oxidoreductase of higher plants. Isolation and characterization of the bc1 complex from potato tuber mitochondria." *J Biol Chem* **266**: 9064-77.
- Berry EA, Huang LS, Zhang ZL and Kim SH (1999). "Structure of the avian mitochondrial cytochrome bc(1) complex." *Journal of Bioenergetics and Biomembranes* **31**: 177-190.
- Brasseur G, Saribas AS and Daldal F (1996). "A compilation of mutations located in the cytochrome b subunit of the bacterial and mitochondrial bc1 complex." *Biochim Biophys Acta* **1275**: 61-9.
- Brunger AT (1992). "The Free R value: a novel statistical quantity for assessing the accuracy of crystal structures." *Nature* **355**: 472-474.
- Brunger AT, Adams PD, Clore GM, DeLano WL, Gros P, Grosse-Kunstleve RW, Jiang JS, Kuszewski J, Nilges M, Pannu NS, Read RJ, Rice LM, Simonson T and Warren GL (1998). "Crystallography & NMR system: A new software suite for macromolecular structure determination." *Acta Crystallogr D Biol Crystallogr* **54**: 905-21.
- Carrell CJ, Zhang HM, Cramer WA and Smith JL (1997). "Biological identity and diversity in photosynthesis and respiration: structure of the lumen-side domain of the chloroplast Rieske protein." *Structure* **5**: 1613-1625.
- COLLABORATIVE COMPUTATIONAL PROJECT N (1994). "The CCP4 Suite: Programs for Protein Crystallography". *Acta Cryst. D* **D50**: 760-763.
- Combet C, Blanchet C, Geourjon C and Deleage G (2000). "NPS@: network protein sequence analysis." *Trends Biochem Sci* **25**: 147-50.
- Cooley JW, Roberts AG, Bowman MK, Kramer DM and Daldal F (2004). "The raised midpoint potential of the [2Fe2S] cluster of cytochrome bc1 is mediated by both the Qo site occupants and the head domain position of the Fe-S protein subunit." *Biochemistry* **43**: 2217-27.
- Cramer WA, Soriano GM, Ponomarev M, Huang D, Zhang H, Martinez SE and Smith JL (1996). "Some new structural aspects and old controversies concerning the cytochrome b(6)f complex of oxygenic photosynthesis." *Annual Review of Plant Physiology and Plant Molecular Biology* **47**: 477-508.
- Cramer WA, Zhang H, Yan JS, Kurisu G and Smith JL (2004). "Evolution of Photosynthesis: Time-independent structure of the cytochrome b6f complex of oxygenic photosynthesis." *Biochemistry* **in press**.
- Crofts AR, Guergova-Kuras M, Kuras R, Ugulava N, Li JY and Hong SJ (2000). "Proton-coupled electron transfer at the Q(o) site: what type of mechanism can account for the high activation barrier?" *Biochimica Et Biophysica Acta-Bioenergetics* **1459**: 456-466.
- Crofts AR and Meinhardt SW (1982). "A Q-Cycle Mechanism for the Cyclic Electron-Transfer Chain of Rhodospseudomonas-Sphaeroides." *Biochemical Society Transactions* **10**: 201-203.
- Crofts AR, Meinhardt SW, Jones KR and Snozzi M (1983). "The Role of the Quinone Pool in the Cyclic Electron-Transfer Chain on Rhodospseudomonas-Sphaeroides - a Modified Q-Cycle Mechanism." *Biochimica Et Biophysica Acta* **723**: 202-218.
- Crowley PB, Vintonenko N, Bullerjahn GS and Ubbink M (2002). "Plastocyanin-cytochrome f interactions: The influence of hydrophobic patch mutations studied by NMR

- spectroscopy." *Biochemistry* **41**: 15698-15705.
- Darrrouzet E, Cooley JW and Daldal F (2004). "The cytochrome bc(1) complex and its homologue the b(6)f complex: similarities and differences." *Photosynthesis Research* **79**: 25-44.
- Darrrouzet E, Moser CC, Dutton PL and Daldal F (2001). "Large scale domain movement in cytochrome bc(1): a new device for electron transfer in proteins." *Trends in Biochemical Sciences* **26**: 445-451.
- Darrrouzet E, Valkova-Valchanova M, Moser CC, Dutton PL and Daldal F (2000). "Uncovering the 2Fe2S domain movement in cytochrome bc(1) and its implications for energy conversion." *Proceedings of the National Academy of Sciences of the United States of America* **97**: 4567-4572.
- Degli Esposti M, De Vries S, Crimi M, Ghelli A, Patarnello T and Meyer A (1993). "Mitochondrial cytochrome b: evolution and structure of the protein." *Biochim Biophys Acta* **1143**: 243-71.
- di Rago JP, Sohm F, Boccia C, Dujardin G, Trumpower BL and Slonimski PP (1997). "A point mutation in the mitochondrial cytochrome b gene obviates the requirement for the nuclear encoded core protein 2 subunit in the cytochrome bc1 complex in *Saccharomyces cerevisiae*." *J Biol Chem* **272**: 4699-704.
- Diederichs K and Karpus PA (1997). "Improved R-factors for diffraction data analysis in macromolecular crystallography." *Nat Struct Biol* **4**: 269-75.
- Gao X, Wen X, Esser L, Quinn B, Yu L, Yu CA and Xia D (2003). "Structural basis for the quinone reduction in the bc(1) complex: a comparative analysis of crystal structures of mitochondrial cytochrome bc(1) with bound substrate and inhibitors at the Q(i) site." *Biochemistry* **42**: 9067-80.
- Hochkoeppler A, Zannoni D, Ciurli S, Meyer TE, Cusanovich MA and Tollin G (1996). "Kinetics of photo-induced electron transfer from high-potential iron-sulfur protein to the photosynthetic reaction center of the purple phototroph *Rhodospirillum rubrum*." *Proceedings of the National Academy of Sciences of the United States of America* **93**: 6998-7002.
- Hunsicker-Wang LM, Heine A, Chen Y, Luna EP, Todaro T, Zhang YM, Williams PA, McRee DE, Hirst J, Stout CD and Fee JA (2003). "High-resolution structure of the soluble, respiratory-type Rieske protein from *Thermus thermophilus*: analysis and comparison." *Biochemistry* **42**: 7303-7317.
- Hunte C, Koepke J, Lange C, Rossmann T and Michel H (2000). "Structure at 2.3 Å resolution of the cytochrome bc(1) complex from the yeast *Saccharomyces cerevisiae* co-crystallized with an antibody Fv fragment." *Structure Fold Des* **8**: 669-84.
- Iwata S, Lee JW, Okada K, Lee JK, Iwata M, Rasmussen B, Link TA, Ramaswamy S and Jap BK (1998). "Complete structure of the 11-subunit bovine mitochondrial cytochrome bc1 complex [see comments]." *Science* **281**: 64-71.
- Jenney FE and Daldal F (1993). "A Novel Membrane-Associated C-Type Cytochrome, Cyt C₂, Can Mediate the Photosynthetic Growth of *Rhodospirillum rubrum* and *Rhodospirillum rubrum* Sphaeroides." *Embo Journal* **12**: 1283-1292.
- Jenney FE, Prince RC and Daldal F (1994). "Roles of the Soluble Cytochrome C(2) and Membrane-Associated Cytochrome C(Y) of *Rhodospirillum rubrum* in Photosynthetic Electron-Transfer." *Biochemistry* **33**: 2496-2502.
- Jones TA, Zhou J-Y, Cowan SW and Kjeldgaard M (1991). "Improved methods for building protein models in electron density maps and the location of errors on these models." *Acta Crystallogr.* **A47**: 110-119.
- Kerfeld CA, Chan C, Hirasawa M, KleisSanFrancisco S, Yeates TO and Knaff DB (1996). "Isolation and characterization of soluble electron transfer proteins from *Chromatium purpuratum*." *Biochemistry* **35**: 7812-7818.
- Kleywegt GJ and Jones TA (1994). Convenient single and multiple crystal real-space . . . [CCP4 Newsletter](#): 59-66.
- Kraulis PJ (1991). "MOLSCRIPT: a program to produce both detailed and schematic plots of protein structures." *J. Appl. Crystallogr.* **24**: 946-950.
- Kuras R, Guergova-Kuras M and Crofts AR (1998). "Steps toward constructing a cytochrome b(6)f complex in the purple bacterium *Rhodospirillum rubrum*: An example of the

- structural plasticity of a membrane cytochrome." *Biochemistry* **37**: 16280-16288.
- Kurusu G, Zhang HM, Smith JL and Cramer WA (2003). "Structure of the cytochrome b(6)f complex of oxygenic photosynthesis: Tuning the cavity." *Science* **302**: 1009-1014.
- Kurowski B and Ludwig B (1987). "The Genes of the Paracoccus-Denitrificans-Bc1 Complex - Nucleotide-Sequence and Homologies between Bacterial and Mitochondrial Subunits." *Journal of Biological Chemistry* **262**: 13805-13811.
- Lange C and Hunte C (2002). "Crystal structure of the yeast cytochrome bc1 complex with its bound substrate cytochrome c." *Proc Natl Acad Sci U S A* **99**: 2800-5.
- Martinez SE, Huang D, Szczepaniak A, Cramer WA and Smith JL (1994). "Crystal-Structure of Chloroplast Cytochrome-F Reveals a Novel Cytochrome Fold and Unexpected Heme Ligation." *Structure* **2**: 95-105.
- McFadden DC, Tomavo S, Berry EA and Boothroyd JC (2000). "Characterization of cytochrome b from *Toxoplasma gondii* and Q(o) domain mutations as a mechanism of atovaquone-resistance." *Mol Biochem Parasitol* **108**: 1-12.
- Mitchell P (1976). "Possible molecular mechanisms of the protonmotive function of cytochrome systems." *J Theor Biol* **62**: 327-67.
- Muller F, Crofts AR and Kramer DM (2002). "Multiple Q-cycle bypass reactions at the Q(o) site of the cytochrome bc(1) complex." *Biochemistry* **41**: 7866-7874.
- Navaza J (1994). *Acta Cryst. A* **A50**: 157-163.
- Osyczka A, Dutton PL, Moser CC, Darrouzet E and Daldal F (2001). "Controlling the functionality of cytochrome c(1) redox potentials in the *Rhodobacter capsulatus* bc(1) complex through disulfide anchoring of a loop and a beta-branched amino acid near the heme-ligating methionine." *Biochemistry* **40**: 14547-14556.
- Osyczka A, Moser CC, Daldal F and Dutton PL (2004). "Reversible redox energy coupling in electron transfer chains." *Nature* **427**: 607-612.
- Otwinowski Z, Borek D, Majewski W and Minor W (2003). "Multiparametric scaling of diffraction intensities." *Acta Crystallogr A* **59**: 228-34.
- Palsdottir H, Lojero CG, Trumpower BL and Hunte C (2003). "Structure of the Yeast Cytochrome bc1 Complex with a Hydroxyquinone Anion Qo Site Inhibitor Bound." *J Biol Chem* **278**: 31303-31311.
- Rieske JS, MacLenna DH and Coleman R (1964). "Isolation + Properties of Iron-Protein from Beef Heart Mitochondria." *Federation Proceedings* **23**: 323-&.
- Robertson DE, Ding HG, Chelminski PR, Slaughter C, Hsu J, Moomaw C, Tokito M, Daldal F and Dutton PL (1993). "Hydroubiquinone Cytochrome-C2 Oxidoreductase from *Rhodobacter-Capsulatus* - Definition of a Minimal, Functional Isolated Preparation." *Biochemistry* **32**: 1310-1317.
- Saribas AS, Mandaci S and Daldal F (1999). "An engineered cytochrome b(6)c(1) complex with a split cytochrome b is able to support photosynthetic growth of *Rhodobacter capsulatus*." *Journal of Bacteriology* **181**: 5365-5372.
- Sayle RA and Milner-White EJ (1995). "RASMOL: biomolecular graphics for all." *Trends Biochem Sci* **20**: 374.
- Schagger H, Brandt U, Gencic S and von Jagow G (1995). "Ubiquinol-cytochrome-c reductase from human and bovine mitochondria." *Methods Enzymol* **260**: 82-96.
- Soriano GM, Ponamarev MV, Carrell CJ, Xia D, Smith JL and Cramer WA (1999). "Comparison of the cytochrome bc1 complex with the anticipated structure of the cytochrome b6f complex: de plus ca change de plus c'est la meme chose [In Process Citation]." *J Bioenerg Biomembr* **31**: 201-13.
- Stonehuerner J, O'Brien P, Geren L, Millett F, Steidl J, Yu L and Yu CA (1985). "Identification of the Binding-Site on Cytochrome-C1 for Cytochrome-C." *Journal of Biological Chemistry* **260**: 5392-5398.
- Stroebel D, Choquet Y, Popot JL and Picot D (2003). "An atypical haem in the cytochrome b(6)f complex." *Nature* **426**: 413-418.
- Trumpower BL (2002). "A concerted, alternating sites mechanism of ubiquinol oxidation by the dimeric cytochrome bc(1) complex." *Biochimica Et Biophysica Acta-Bioenergetics* **1555**: 166-173.
- Xia D, Yu CA, Kim H, Xian JZ, Kachurin AM, Zhang L, Yu L and Deisenhofer J (1997). "Crystal

- structure of the cytochrome bc(1) complex from bovine heart mitochondria (vol 277, pg 60, 1997)." *Science* **278**: 2037-2037.
- Xiao KH, Liu XY, Yu CA and Yu L (2004). "The extra fragment of the iron-sulfur protein (residues 96-107) of *Rhodobacter sphaeroides* cytochrome bc(1) complex is required for protein stability." *Biochemistry* **43**: 1488-1495.
- Yang XH and Trumpower BL (1986). "Purification of a three-subunit ubiquinol-cytochrome c oxidoreductase complex from *Paracoccus denitrificans* [published erratum appears in *J Biol Chem* 1986 Nov 25;261(33):15813]." *J Biol Chem* **261**: 12282-9.
- Yun CH, Crofts AR and Gennis RB (1991). "Assignment of the histidine axial ligands to the cytochrome bH and cytochrome bL components of the bc1 complex from *Rhodobacter sphaeroides* by site-directed mutagenesis." *Biochemistry* **30**: 6747-54.
- Zara V, Palmisano I, Conte L and Trumpower BL (2004). "Further insights into the assembly of the yeast cytochrome bc(1) complex based on analysis of single and double deletion mutants lacking supernumerary subunits and cytochrome b." *European Journal of Biochemistry* **271**: 1209-1218.
- Zhang Z, Huang L, Shulmeister VM, Chi YI, Kim KK, Hung LW, Crofts AR, Berry EA and Kim SH (1998). "Electron transfer by domain movement in cytochrome bc1." *Nature* **392**: 677-84.

Figure Legends

Figure 1. Structures of mitochondrial, bacterial and chloroplast cyt bc_1 /cyt b_6f complexes. Bovine heart (left), *Rb. capsulatus* (middle) and *C. reinhardtii* (right) enzymes are shown with their cyt b , cyt c_1 or cyt f and FeS protein subunits colored in blue, green and yellow, respectively. The other subunits of the mitochondrial and the chloroplast enzymes are shown in gray, and red highlighted regions correspond to the differences between these enzymes. The energy transducing membrane is represented in brown and its P and N sides are indicated.

Figure 2. Comparison of mitochondrial, bacterial and chloroplast cyt b or cyt b_6 and IV subunits. A. Cyt b or b_6 and IV subunits of the yeast mitochondrial, *Rb. capsulatus*, and *C. reinhardtii* enzymes are shown from left to right. The Rieske [2Fe2S] cluster and the cyt f/c_1 heme are also shown to indicate their respective orientations. In the case of *R. capsulatus* cyt b the portions shown in red and numbered from 1 to 5 correspond to the regions that differ from its mitochondrial or chloroplast counterparts, and are described in detail in the text. The C and N termini are labeled, with separate labels for the b_6 and subunit IV chains of cyt b_6f . (B. removed in preparation) C. Sequence alignment of cytochromes b/b_6 .

Figure 3. Comparison of horse heart mitochondrial cyt c and cyt c_1 and bacterial cyt c_1 . A. The structures of these three class-I c -type cyts are shown from left to right as indicated on the figure. The structures are oriented in such a way that the solvent exposed face of the heme occupies the same position so that their similar core structure is evident. The regions highlighted in red in the case of horse cyt c and bacterial cyt c_1 , indicate salient differences between these proteins and are discussed in detail in the text. The disulfide bond present in *Rb. capsulatus* cyt c_1 and bovine "hinge protein" (colored in pink) are shown in yellow. B. The *Rb capsulatus* cytochrome from another orientation and in the context of the rest of the complex. The "second membrane anchor" is indicated. C. Sequence alignment in some of the critical regions. A more complete alignment is available in supplemental materials.

Figure 4. Comparison of mitochondrial, bacterial and chloroplast FeS protein subunits. A. The FeS subunits of the cyt bc_1 and b_6f from *Bos taurus*, *Rb capsulatus* and *Mastigocladus laminosus* are shown from left to right, respectively. The [2Fe2S] cluster in each case is represented in yellow and orange on the tip of the extrinsic domain of the FeS subunit, and in the mitochondrial and bacterial FeS proteins the regions highlighted in red are discussed in the text in detail. B. Slab through transmembrane region showing the different angles of passage of the different FeS protein transmembrane helices. The gray swath represents the membrane, with P side and FeS N-terminus below and the P side and FeS extrinsic domain above. C. Sequence alignment in some of the critical regions. A more complete alignment is available in supplemental materials. D. Spacefilling model of the bacterial FeS extrinsic domain, seeing the end away from the cluster, with the atoms comprising inserts 2 and 3 colored magenta (stereo pair).

Figure 1
[Click here to download high resolution image](#)

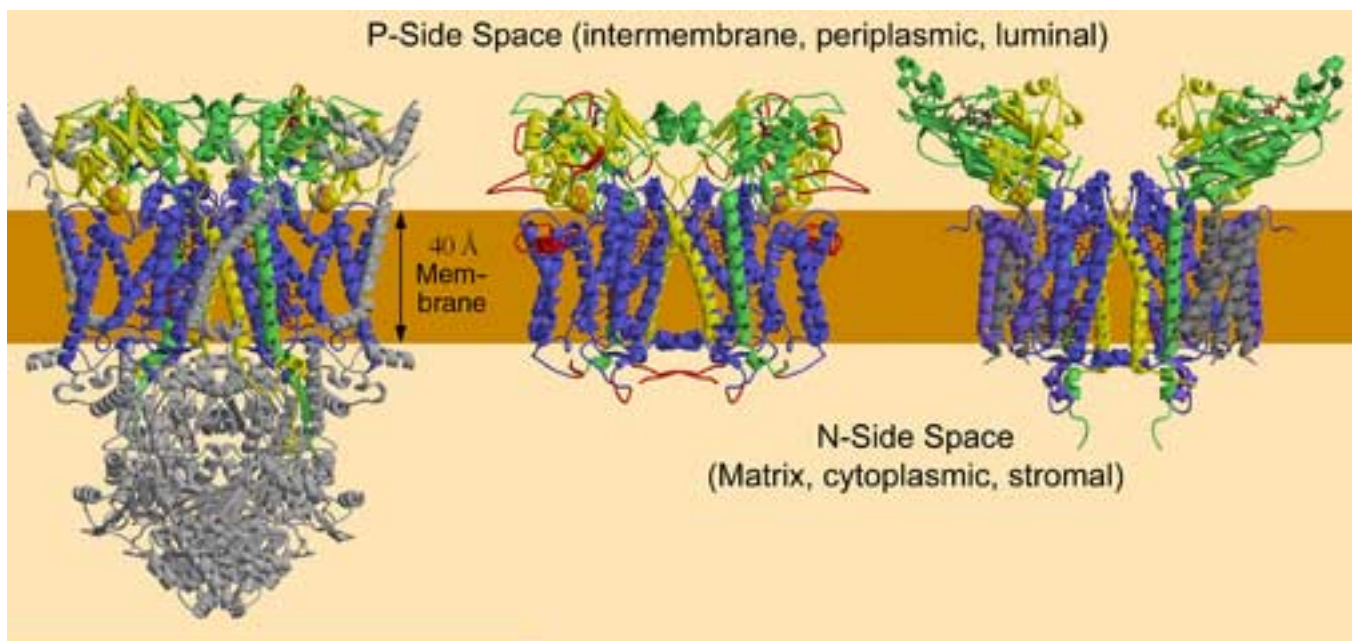


Figure 2A
[Click here to download high resolution image](#)

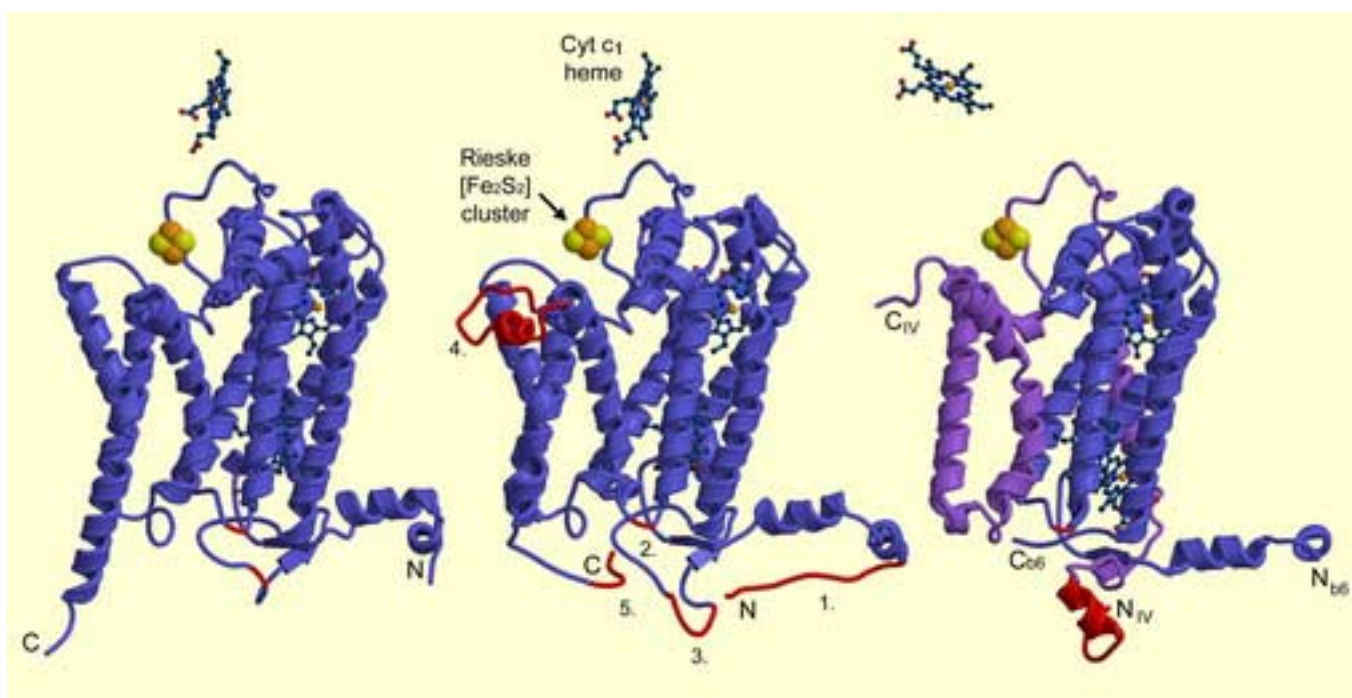


Figure 2C

	110	120	130	140	150	160
Rhbactersphaer	SYKAPREVTWIVGMLIYLAMMATAFMGYVLPWGQMSFWGATVITGLFGAIPGIGHSIQTW					
Paracoccus	SYKAPREVTWIVGMLIYLLMMGTAFMGYVLPWGQMSFWGATVITGLFGAIPGVGEAIQTW					
Rbcapsul	SYKAPREITWIVGMVIYLLMMGTAFMGYVLPWGQMSFWGATVITGLFGAIPGIGPSIQAW					
Bostaurus	SYT--FLETWNIQVILLLLTVMATAFMGYVLPWGQMSFWGATVITNLLSAIPYIGTNLVEW					
chicken	SYL--YKETWNTGVILLLLTLMATAFVGYVLPWGQMSFWGATVITNLFSAIPYIGHTLVEW					
Saccharocere	SYRSPRVTLWNVGVIFILTIATAFLGYCCVYGQMSHWGATVITNLFSAIPFVGNDIVSW					
	170	180	190	200	210	
Rhbactersphaer	LLGGPAVDNATLNRFFSLHYLLPFVIAALVAIHIWAFHSTGNNNPTGVEVRRTSKAEQAQK					
Paracoccus	LLGGPAVDNPTLNRFFSLHYLLPFVIAALVVVHIWAFHTTGNNNPTGVEVRRGSKEEAKK					
Rbcapsul	LLGGPAVDNATLNRFFSLHYLLPFVIAALVAIHIWAFHTTGNNNPTGVEVRRTSKADAQK					
Bostaurus	IWGGFSVDKATLTRFFAFHFILPFIIMAIAMVHLLFLHETGSSNPTGISS-----DV-					
chicken	AWGGFSVDNPTLTRFFALHFLLPFAIAGITIIHLTFLHESGSSNPLGISS-----DS-					
Saccharocere	LWGGFSVSNPTIQRFFALHYLVPFIIAAMVIMHLMALHIHGSSNPLGITG-----NL-					
	220	230	240	250	260	270
Rhbactersphaer	DTVPFWPYFIIKDVIFALAVVLLVFFAIVGFMPNYLGHPDNYIEANPLSTPAHIVPEWYFL					
Paracoccus	DTLPFWPYFVIKDLFALAVVLLVFFAIVGFMPNYLGHPDNYIEANPLVTPAHIVPEWYFL					
Rbcapsul	DTLPFWPYFVIKDLFALALVLLGFFAVVAYMPNYLGHPDNYVQANPLSTPAHIVPEWYFL					
Bostaurus	DKIIPFHPYTIKDIILGALLLILALMLLVLFPDLDGDPDNYTPANPLNTPPHIKPEWYFL					
chicken	DKIIPFHPYYSFKDIILGLTLMFLTPFLTLALFSPNLLGDPENFTPANPLVTPPHIKPEWYFL					
Saccharocere	DRIPMHSYFIFKDLVTVFLFMLLILALFVYFSPNTLQGPDNYIPGNPLVTPASIDPEWYLL					
	280		290	300	310	
Rhbactersphaer	PFYAILRAFTADVWVQIANFISFGIIDAKKFFGVILAMFGAILVMALVPWLDTSRVRSGRY					
Paracoccus	PFYAILRAFTADVWVMLVNWLSFGIIDAKKFFGVILAMFGAILVMALVPWLDTSRVRSGQY					
Rbcapsul	PFYAILRAFAADVWVILVDGLTFGIVDAKFFGVILAMFGAIVMALVPWLDTSKVRSGAY					
Bostaurus	FAYAILRS-----IPNKLGGVLAALAFSILILALIPLLHTSKQRSMMF					
chicken	FAYAILRS-----IPNKLGGVLAALAAASVLILFLIPFLHKSQRMTTF					
Saccharocere	PFYAILRS-----IPDKLLGVITMFAAILVLLVLPFTDRSVVRGNTF					
	320	330	340	350	360	370
Rhbactersphaer	RPMFKIYFWLLAADFVILTWVGAQQTTFPYDWISLIASAYWFAYFLVILPILGAIKPVPA					
Paracoccus	RPLFKWFWLLAVDFVLLMWVGAMPAEGIYPYIALAGSAYWFAYFLIILPLLGIIEKPDA					
Rbcapsul	RPKFRMFWFLVLDVFLTWVGAQTEYPYDWISLIASTYWFAYFLVILPILGATEKPEP					
Bostaurus	RPLSQCLFWALVADLLTLTWIGGQPVHEHPYITIGQLASVLYFLLIILVLMPTAGTIENKLL					
chicken	RPLSQTLFWLLVANLLLILTWIGSQPVHEHPYITIGQMASLSYFTILLIILPFTIGTLENKML					
Saccharocere	KVLSKFFFIFVFNFLVLLGQIGACHVEVPYVLMGQIATFIYFAYFLIIVPVIETIENVLF					
	380	390	400			
Rhbactersphaer	PPATIEEDFNAHYSPATGGTKTVVAE					
Paracoccus	MPQTIEEDFNAHYGPETHPAE-----					
Rbcapsul	IPASIEEDFNSHYG---NPAE-----					
Bostaurus	KW-----					
chicken	NY-----					
Saccharocere	YIGRVNK-----					

Figure 3A

[Click here to download high resolution image](#)

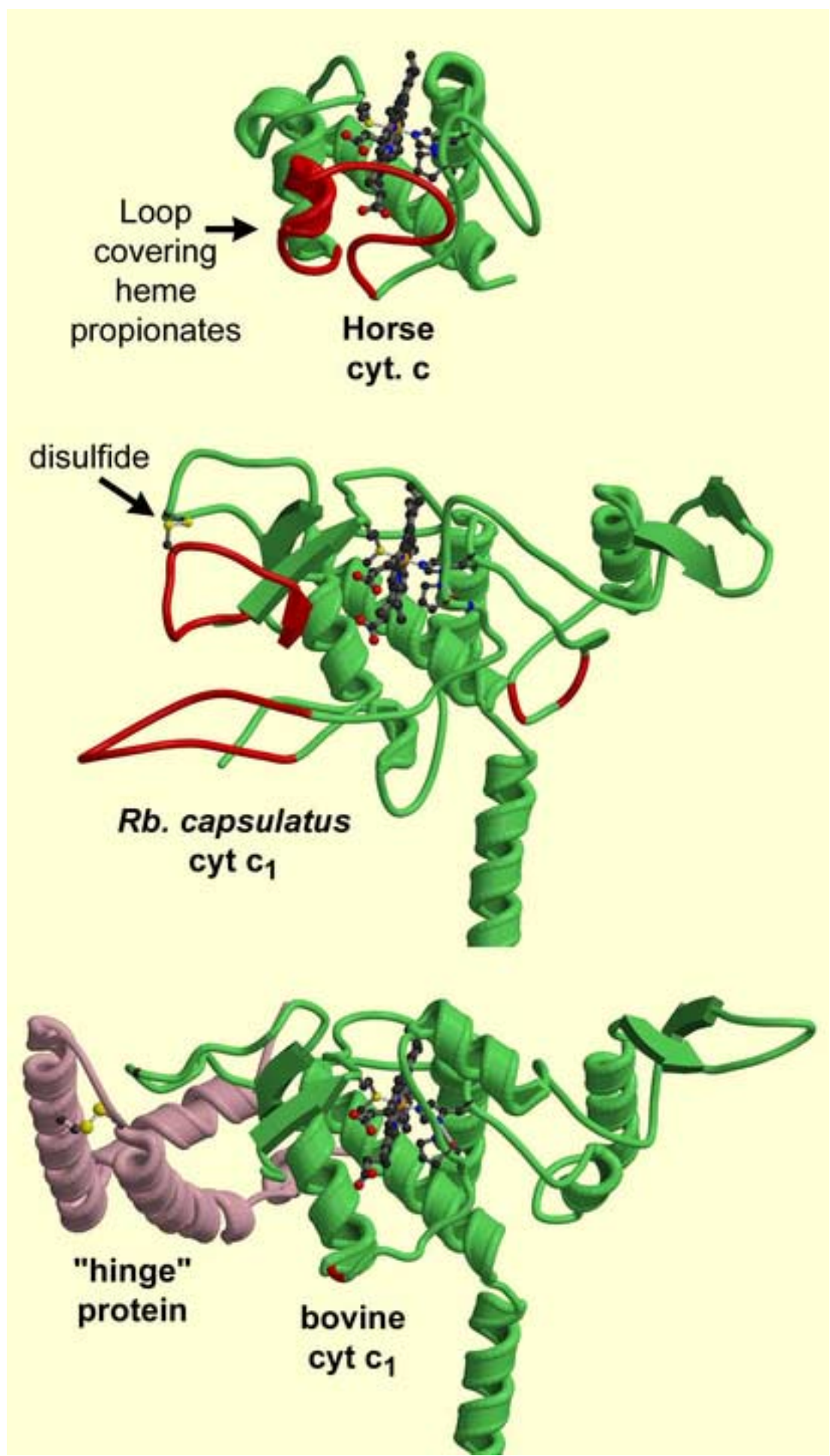


Figure 3B
[Click here to download high resolution image](#)

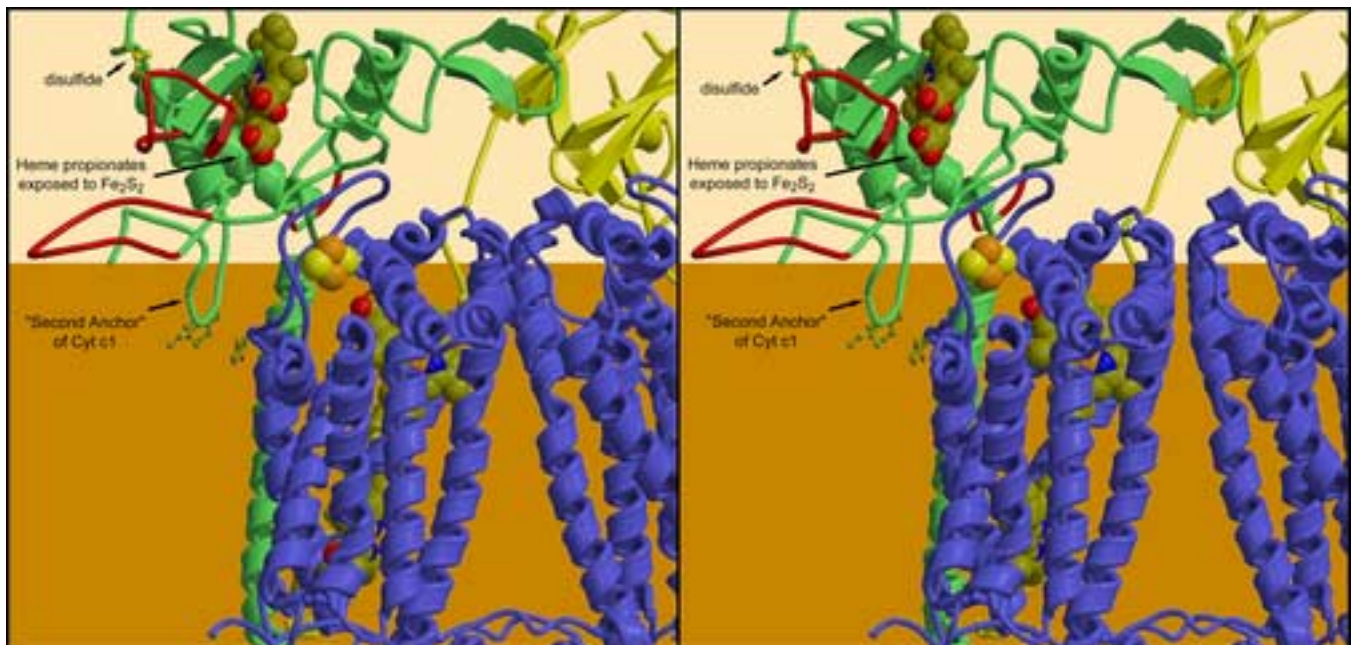


Figure 3C (eps)

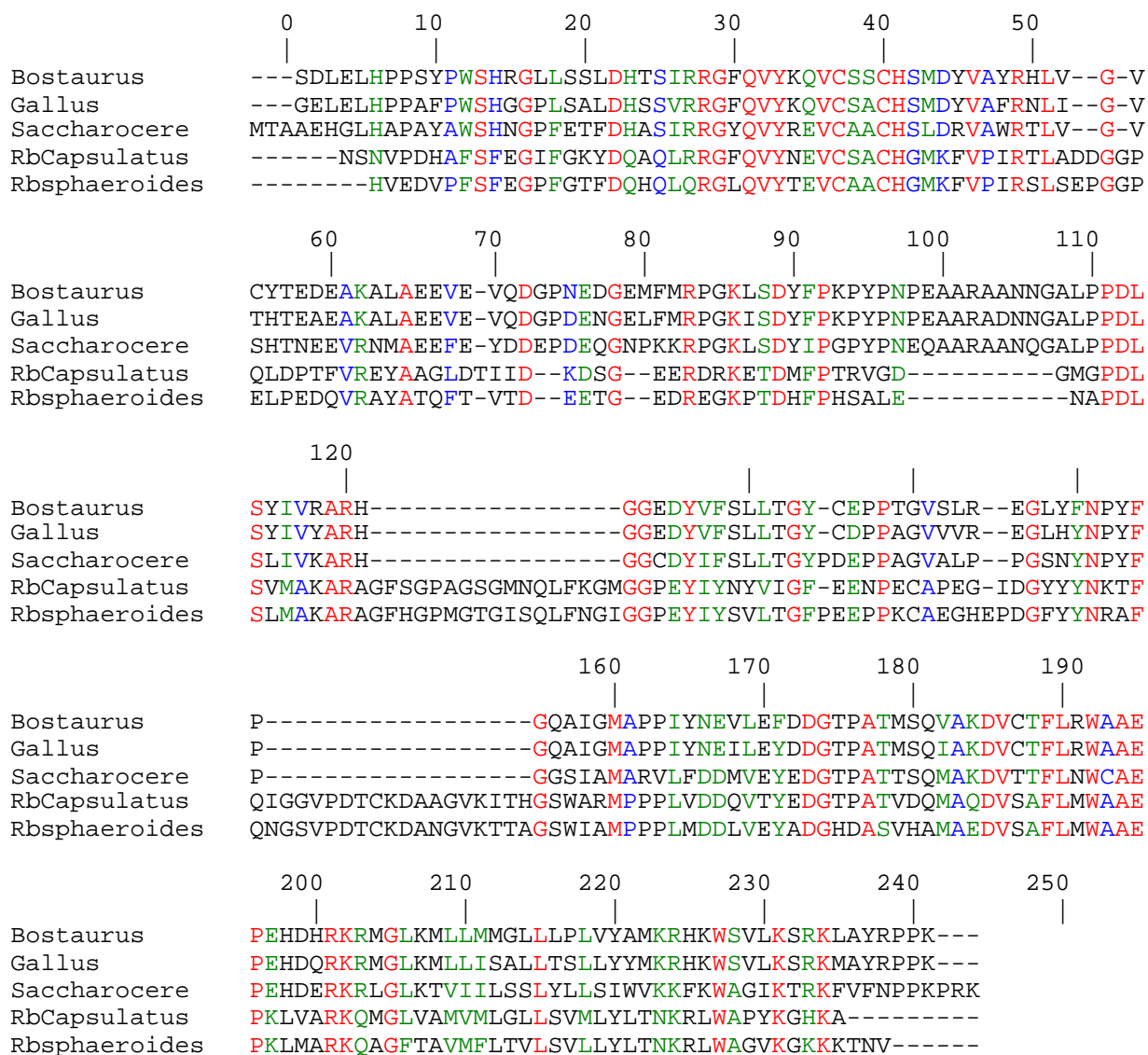


Figure 4A
[Click here to download high resolution image](#)

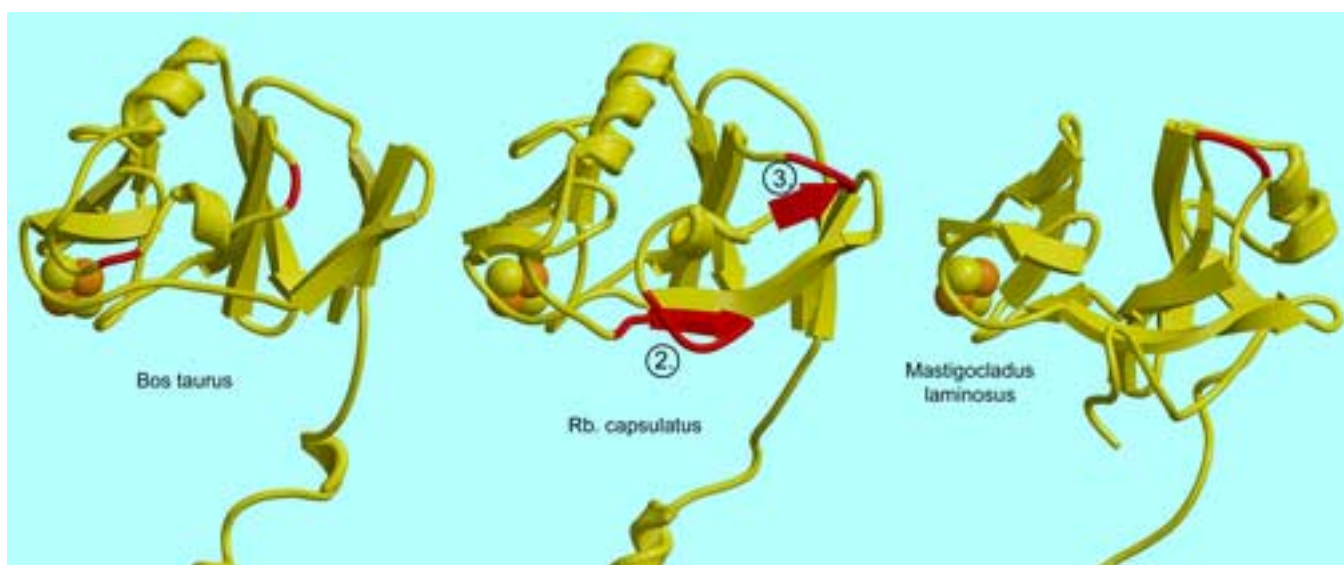


Figure 4B

[Click here to download high resolution image](#)

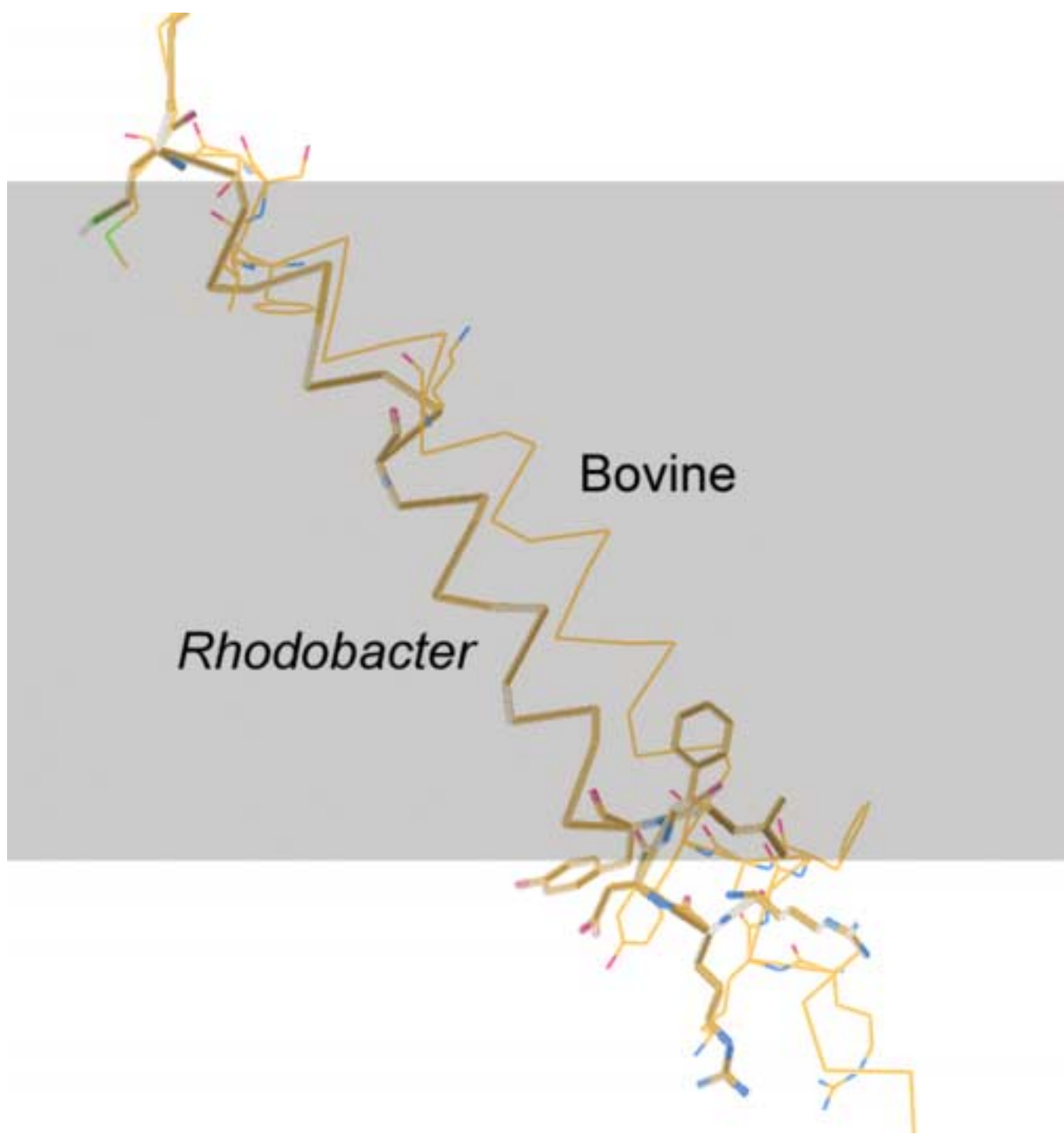


Figure 4C (EPS)

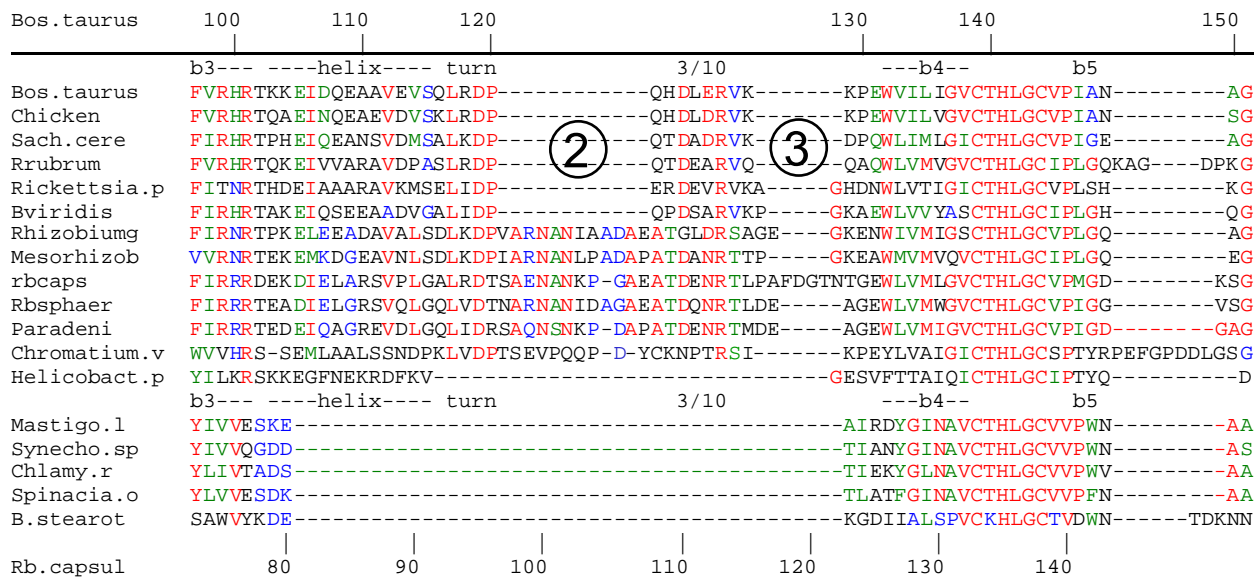
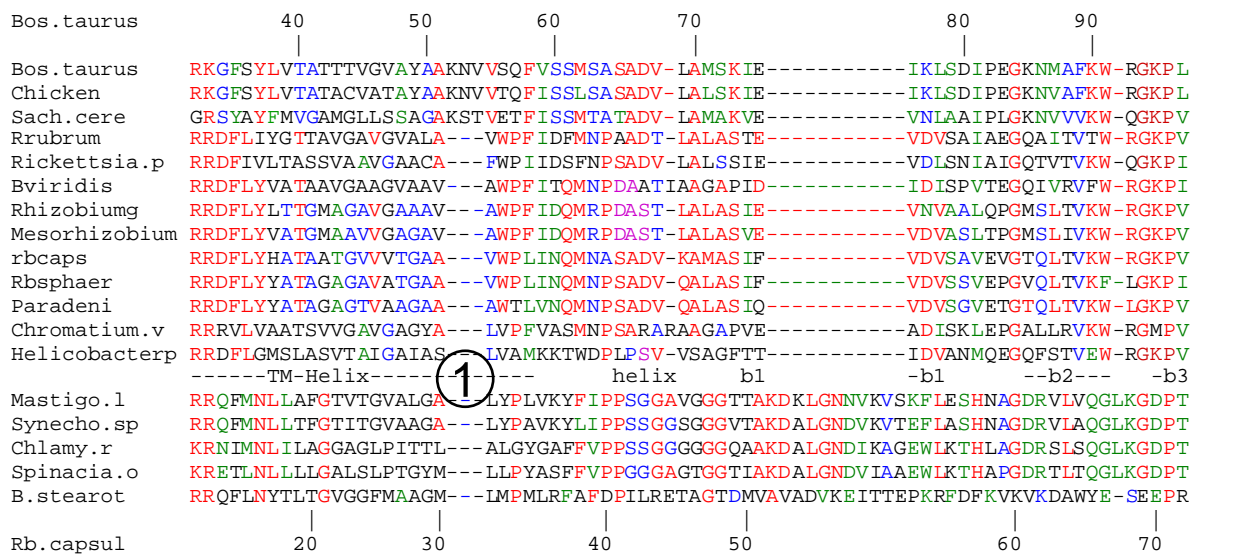


Figure 4D
[Click here to download high resolution image](#)

